

DROUGHT MONITORING AND ASSESSMENT USING REMOTE SENSING

MUIRURI PETER MAINA

March 2018

SUPERVISORS:

Prof. Z. Su.

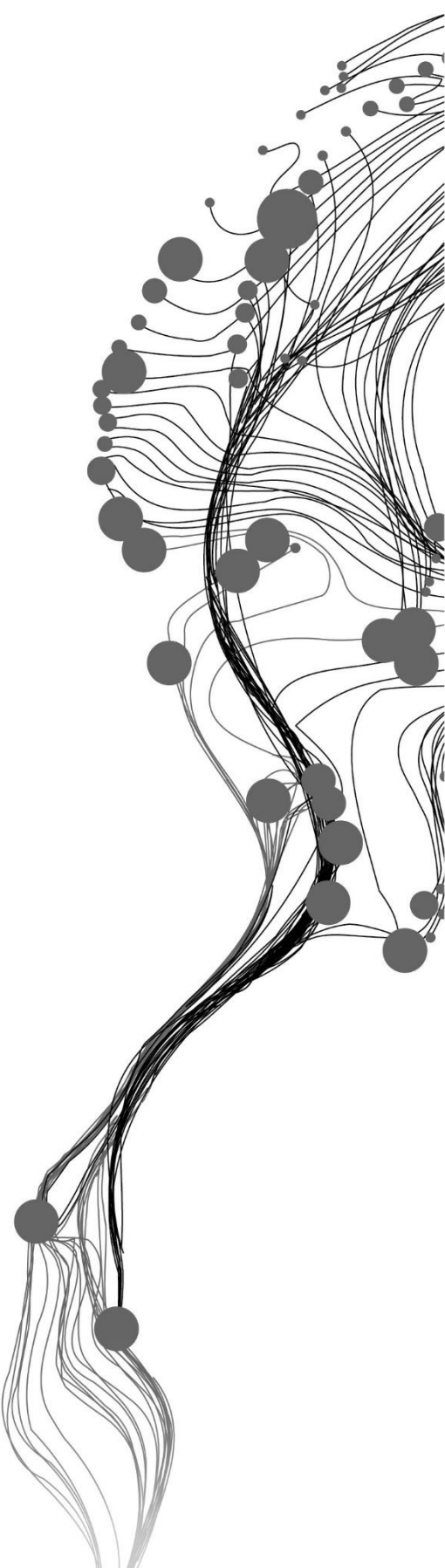
Dr. Christiaan van der Tol

Dr. Chen Xuelong

THESIS ASSESSMENT BOARD:

Dr. C .M .M. Mannaerts (Chair)

Prof. Dr. M. Menenti (External Examiner, Capital Normal University
(CNU), Beijing, China)



DROUGHT MONITORING AND ASSESSMENT USING REMOTE SENSING

MUIRURI PETER MAINA

Enschede, The Netherlands, March 2018

Thesis submitted to the Faculty of Geo-Information Science and Earth Observation of the University of Twente in partial fulfilment of the requirements for the degree of Master of Science in Geo-information Science and Earth Observation.

Specialization: Water Resources Management

SUPERVISORS:

Prof. Dr. Z. Su

Dr. Christiaan van der Tol

Dr. Chen Xuelong (Advisor)

THESIS ASSESSMENT BOARD:

Dr. C .M .M. Mannaerts (Chair)

Prof. Dr. M. Menenti (External Examiner, Capital Normal University (CNU), Beijing, China)

DISCLAIMER

This document describes work undertaken as part of a programme of study at the Faculty of Geo-Information Science and Earth Observation of the University of Twente. All views and opinions expressed therein remain the sole responsibility of the author, and do not necessarily represent those of the Faculty.

ABSTRACT

In order to harmonize how drought is monitored and reduce inconsistencies occasioned by the lack of a universal standard to measure and characterize drought, Su, He et al. (2017) proposed a framework of standardized drought indices: the standardized precipitation index (SPI), standardized precipitation and evapotranspiration index (SPEI), standardized vegetation index (SVI), SDSI-ETDI and the standardized terrestrial water storage index (STWSI), able to describe all the aspects of drought, the onset duration, severity, spread and concurrently address the three forms of drought, agricultural, meteorological and hydrological drought. The framework is anchored on similar standardization method to make the inputs and the indices comparable and compatible.

This research focused on the Yangze River Basin, China to test whether the approach of Su is applicable or not, and whether it really gives a complete understanding of drought events. In determining SPEI, a modified approach introduced by Homdee et al. (2016) was applied instead, effectively substituting SPEI with SPAEI. The research considered a framework of four indices, the SPI, SPAEI, SVI and the STWSI to study drought trends over China from January 2003 to December 2016 using monthly datasets of CHIRPS rainfall, SEBS ETa, MODIS NDVI and the GRACE TWS at 0.05° spatial resolution.

This research adopted the proposed standardized drought indices to establish drought trends over Yangtze River basin using satellite and in-situ data. CHIRPS precipitation data, in-situ river discharge measurements from Cuntan gauging station on R. Yangtze, actual evapotranspiration (ET) estimated from SEBS, vegetation indices from MODIS and terrestrial water storage estimates from the GRACE satellite data is used.

The performance of the indices is assessed graphically and statistically through scatterplots, time series, Pearson correlation coefficients and map-series. The drought indices adequately capture reported drought events and are consistent. However, the SVI pattern is discordant at time steps >9 months and entirely misses key drought events otherwise captured by the SPI, SPAEI or STWSI. STWSI capture drought events at higher magnitude/severity as it is influenced by deep groundwater fluxes.

The indices are positively correlated with each other at all timescales apart from a few instances with the SVI-12 and SVI-24. SPI and SPAEI exhibit good correlation ranging from 0.83-0.97 at similar time steps and is highest at 9-month time step. Both SPI and SPAEI show a weak correlation against the SVI and STWSI at dissimilar timescales ranging from 0.14 to 0.6. Results of a correlation matrix prepared to show basin average inter-indices relationship at different scales suggest the correlation increase at longer time scales (6-12 month time step) and is lowest at 1-month with SPI and SPAEI. Unlike the SPI and SPAEI, SVI and STWSI have maximum correlation at shorter-times (3-month and 1-month) an indication that both respond to well to hydrological cycle changes occurring at shallow depth. SVI show subtle variability across all the time-scales and slow response to meteorological influences. SPI and SPAEI are best correlated at longer-term (and is maximum at >6month SPI/SPAEI when the hydrological cycle changes at depth. The indices simulate the drought tendencies well and capture drought events consistent with documented reports and research.

Although there is no water balance closure in the basin, the results of the catchment water balance are comparable. The PBIAS between the accumulated mean annual observed discharge against the calculated runoff is small (8.85%), despite considerable month-month differences. Further, the deficits in the water balance appear to have a four-year repeat cycle occur just before (coincide with) reported drought events. Notably, amount of water released from the Three Gorge Dam appear to be less than normal observed

discharges in the subsequent year. If not coincidental, this confirms Su, He, et al.(2017) assertion that, the water balance can infer drought.

The proposed framework is feasible and adaptable and can offer integral alternatives as to how drought monitoring is done. However further research testing is needed. Future research should incorporate in-situ measurements and an appropriate hydrological model and soil moisture data.

Keywords: Drought, Standardized Drought Index, Standardized Precipitation Index, Precipitation, Evapotranspiration, Remote Sensing, Terrestrial Water Storage, GRACE

Dedication

.....to Bill, Gladys, Mum and Dad.

ACKNOWLEDGEMENT

It is through God that this has been accomplished! Glory and honor to him.

Secondly, to the Dutch government, through the Netherlands Fellowship Program (NFP), for funding and for the opportunity to further my studies. Along with the exposure, it has been an awesome experience.

To my family, thank you for your support, prayers and encouragement despite being away from you for so long. Special mention to my spouse Gladys for believing in me despite my inadequacies, your support, sacrifice and for being there for us and Bill.

To my supervisors thank you for being patient with me and for guiding me through. To Dr. Christiaan Van der Tol, off your busy schedule, you always had time for me when I came to you even without an appointment. You accommodated and understood me. Your valuable input and help with programming made this research a success. Thank you. To my advisor Dr. Chen Xuelong, you have been like an elder brother to me. When it seemed foggy and frosty, you illuminated the way. Thank you for the data and insight. To Prof. Bob Su, you inspired me and you have been a yardstick for excellence. To Sammy Njuki, Donald Rwasoka and Calisto Kennedy, the discussions we had were really helpful and very much appreciated.

To my confidant and friend Caroline Ngunjiri, this would have not possible without your facilitation. I remain indebted to you.

Also, I would like to sincerely thank to my direct line managers and mentors, Scott Gilmour and Luc Joos-Vandewalle, at Schlumberger Kenya for approving my request for study leave and helping with career progression and transition logistics.

To Aman, Aldino and Harm, thank you immensely for the help with MATLAB.

Special thanks to John Mutinda, Ken Wekesa, Amos Tabalia and Kyalo for encouraging me to further my studies, friendship and support.

To all my classmates and colleagues, Makau, Irene, Raazia, Roudan, Sam, and Muketiwa, despite the storm, tides, and shoals, with resilience, it is done!

TABLE OF CONTENTS

List of figures	vi
List of tables	vii
List of Appendices.....	viii
Acronyms.....	ix
1. Introduction.....	1
1.1. Background.....	1
1.2. Research problem	2
1.3. Justification	2
1.4. Research objectives and Questions	2
2. Theoretical background.....	4
2.1. Drought.....	4
2.2. Drought related studies in China.....	6
2.3. The standardized drought indices.....	6
3. Study area and data.....	13
3.1. Study area.....	13
3.2. Data.....	15
4. Methodology.....	19
4.1. Data processing.....	20
4.2. Standardised Drought Indices Calculation	22
4.3. Time series, scatterplot and the qq-plots.....	23
4.4. Statistical Analysis.....	23
4.5. Water Balance Estimation.....	23
5. Results and discussion.....	25
5.1. Precipitation, ET, TWS, SM and NDVI pattern	25
5.2. Quality control.....	27
5.3. Comparison of the SPI, SPAEI, SVI and STWSI	30
5.4. Drought Assessment: Spatio-temporal drought evolution	35
5.5. Water Balance.....	38
6. Conclusion	41
6.1. Recommendations:.....	42
List of references	43
Appendices	48

LIST OF FIGURES

Figure 2-1: Interrelationships between meteorological, agricultural, hydrological and socio-economic drought (Wilhite & Glantz, 1985).....	4
Figure 3-1: Study area	13
Figure 3-2: The GRACE twin satellites orbiting the earth at an altitude of 500 km and at 220 km distance apart. (University of Texas Center for Space Research).	17
Figure 3-3: GRACE level 3 data of Terrestrial water storage for April 2003.....	18
Figure 4-1: Methodology.....	19
Figure 4-2: Datasets used to calculate the indices and estimate water balance	19
Figure 4-3: Empirical CDF before and after applying the Gaussian filter.....	20
Figure 4-4: TWS before and after spatial interpolation.....	21
Figure 4-5: Cuntan station precipitation time series, 1981-2017	21
Figure 4-6: Elevation map of the Jinsha, Mintuo, and Jialing sub-basins located in the upper reaches of the Yangtze (Huang et al., 2015)	24
Figure 5-1: Basin mean-annual monthly changes in P, ET, TWS, RO, NDVI and SM over the Yangtze Basin. RO is the calculated runoff from the water balance closure.	25
Figure 5-2: Basin mean monthly precipitation, ET, TWS, NDVI and GLDAS SM time series	26
Figure 5-3: SVI variation w.r.t SPI, SPAEI and the STWSI at a pixel within the basin.....	28
Figure 5-4: Time series and histogram fits comparing SVI results obtained using normal standardization to those obtained using standardized the GEV	28
Figure 5-5: Spatial comparison of the calculated SPI-1 and SPAEI-1 to existing SPEI-1 (SPEI database 2015) July 2003 image.....	29
Figure 5-6: A scatter plot showing the correlation between SPI-6 and SPAEI-6, and SVI-6 and QQ-plots showing the distributions. Degrees of freedom in the SPI-STWSI=96; against 166 with SVI and SPAEI.30	
Figure 5-7: Average correlation derived from the correlation matrices by averaging the coefficients at different scales.	31
Figure 5-8: Timeseries of the SPI vs SPAEI from 2003-2016 at pixel (116,330).	32
Figure 5-9: SPI, SPAEI, SVI and the STWSI timeseries for Cuntan Gauging Station from 2003-2016....	32
Figure 5-10: Correlation between SPI and SPAEI series	33
Figure 5-11: Timeseries of the SPI, SPAEI, SVI and the STWSI over a fifteen-year period (2003-2016) for the Yangtze River Basin.	34
Figure 5-12: Comparison of drought as captured by the 3, 9 and 24-month indices in Jan 2006	36
Figure 5-13: Comparison of drought as captured by the 3, 9 and 24-month indices in January 2010.....	36
Figure 5-14: Comparison of drought as captured by the 3, 9 and 24-month indices in July 2006	37
Figure 5-15: Comparison of drought as captured by the 3, 9 and 24-month indices in July 2010	37
Figure 5-16: Relationship between TWS, calculated runoff (Rcalc) and discharge measurements (Robs) at Cuntan Gauging station from 2005-2010.....	38
Figure 5-17: Comparison of the mean annual calculated runoff from satellite estimate against the in-situ measurements (Robs) at Cuntan Gauging station from 2005-2010.....	39

LIST OF TABLES

Table 2-1: Classification of SPI values (Mckee et al., 1993)	7
Table 2-2: The SPEI drought categories.....	8
Table 2-3: The SVI drought classification (based on probability of occurrence)	10
Table 2-4: The STWSI drought classification	11
Table 3-1 Datasets characteristics and source.....	15

LIST OF APPENDICES

Appendix 1: Correlation matrix (Part 1).....	48
Appendix 2: Correlation matrix (Part 2).....	49
Appendix 3: The SPI MATLAB script.....	50
Appendix 4: MODIS NDVI empirical cumulative probability distribution.....	51
Appendix 5: Comparison of drought as captured by the 1, 6 and 12-month indices in January 2006 and January 2010.....	52
Appendix 6: Comparison of drought as captured by the 1, 6 and 12-month indices in July 2006 and July 2010	53

ACRONYMS

CHIRPS	Climate Hazards Group Infra-Red Precipitation with station data
DI	Drought Index
DSI	Drought Severity Index
EO	Earth observation data
ET	Evapotranspiration
ETDI	Evapotranspiration Deficit Index
FEWSNET	Famine Early Warning Systems Network
GEV	Generalized Extreme Value probability distribution
GLDAS	Noah Global Land
GPCC	Global Precipitation Climatology Centre
GRACE	Gravity Recovery and Climate Experiment satellite
LAI	Leaf Area Index
MODIS	Moderate Resolution Imaging Spectroradiometer
NASA	National Airspace Agency
NDVI	Normalized Difference Vegetation Index
NIR	Near-Infrared
PDF	Probability Density Function
PDSI	Palmer Drought Severity Index
PREC/L	NOAA's PRECipitation REConstruction over Land
RDI	Reconnaissance Drought Index
SDI	Standardized Drought Index
SDSI	Standardized Drought Severity Index
SEBS	Surface Energy Balance System
SPAETI	Standardized Precipitation Actual Evapotranspiration Index
SPEI	Standardized Precipitation Evaporation Index
SPI	Standardized Precipitation Index
SSI	Standardized Severity Index
STWSI	Standardized Terrestrial Water Storage Index
TIR	Thermal-Infrared
TWS	Terrestrial Water Storage
USGS	United States Geological Society
VIR	Visible-Infrared

1. INTRODUCTION

1.1. Background

Drought is a multi-faceted phenomenon caused by a shortage of precipitation due to climatic and hydrological shifts (Su, He, et al., 2017). It is a highly variable, recurrent and a global phenomenon responsible for a myriad of widespread environmental and socio-economic problems such as reduced agricultural productivity, declining water levels, increased wildfire hazards, conflicts and war, death of wildlife and humans among others.

Drought-related effects have adverse financial and social implications and are amongst the most expensive and damaging weather-related events (Yurekli & Kurunc, 2006). In the sub-Saharan Africa for instance, seventeen countries experienced drought between 2015 and 2017 and affected at least 38 million people (Anyadike, 2017). According to recent reports on global food crises, conflict and drought, drought is the main contributor to regional human conflict and war in different parts of the world, especially in Africa, Asia and the Middle East (FAO, IFAD, UNICEF, WFP, & WHO, 2017). China too has experienced drought at varied times in the recent past, with the 2006/2007 and 2009/2010-2011 droughts reported as the worst in the recent past and led to the closure of major sea-routes and canals causing losses running into several billions of dollars (Xu et al., 2015; Yu, Li, Hayes, Svoboda, & Heim, 2014).

Drought is difficult to predict and quantify as it is complex, it manifests gradually, lacks definite onset and depends on several variables. Thus, drought characteristics, intensity and frequency, vary spatially and temporally (Iglesias, Cancelliere, Wilhite, Garrote, & Cubillo, 2009). Drought studies therefore consider various meteorological and land surface parameters to parameterize drought.

Drought has adverse and far-reaching impacts on water resources. Thus, drought assessment and analysis are key to sound water resources management and planning. Distinctively, drought is assessed under meteorological, agricultural, hydrological, and socio-economic aspects using indices (Nagarajan, 2010; Niemeyer, 2008; Wilhite & Glantz, 1985). Over the years, different researchers have proposed different indices to study and monitor drought utilizing both in-situ observations and remote sensing applications. However, attributable to drought variability, for it is a function of precipitation (Heim, 2002; Raziei et al., 2015) and since different satellites give different sensing responses, indices calculated based on the satellite imagery are comparable but differ in interpretation due to inconsistencies in the formulation, estimation and purpose.

To address the inconsistencies, Su, He, et al. (2017) proposed a framework of standardized indices to monitor and assess drought: the standardized precipitation index (SPI; Mckee et al., 1993), the standardized precipitation evaporation index (SPEI; Vicente-Serrano, Beguería, & López-Moreno, 2010), the standardized drought severity index-evapotranspiration index (SDSI-ETDI; Narasimhan & Srinivasan, 2005), the standardized vegetation index (SVI; Peters et al., 2002) and the conceptual standardized terrestrial water storage index (STWSI) to describe meteorological, agricultural and hydrological drought characteristics.

In line with Su, He, et al. (2017) recommendations to assess and monitor drought through a common framework using the five standardized indices or in part, this research sought to find out if the proposed

standardized indices are adaptable and effective. Historic decadal, CHIRPS, GRACE and MODIS satellite imagery was explored to map historical changes in vegetation cover and precipitation variability.

1.2. Research problem

Drought is monitored using drought indices as described in the previous sections. Each index addresses a specific aspect of the water cycle. Over the years, different researchers have formulated different indices to describe the drought characteristics: onset, duration, magnitude and severity. However, there is no universally agreed standard governing formulation, parameterization, interpretation, scope and use. Consequently, an index may show drought while another misses the event for the same area and time. As a result, drought monitoring and assessment becomes ambiguous and involving; often with a constraint on effectiveness, interpretation and integration.

Additionally, having many indices trying to describe the same hydrological phenomenon is counterproductive; and underpins the need to harmonize how drought is monitored; by having one or a set of consistent standardized indices that can effectively define drought: the onset, severity and duration, the spatial-temporal spread and simultaneously address the meteorological, soil moisture and hydrological drought (Su, He, et al., 2017).

As a solution to the problem described in the previous paragraphs, this research is focused on the Yangtze River Basin, China, to test whether the approach of Su, He, et al. (2017) is applicable or not, and whether it really gives a complete understanding of drought events.

1.3. Justification

Some of the significant drought events reported in China between the year 2003 and 2016 include the 2003 short-term drought, the 2006 summer drought, the 2009-2011 drought reported as the worst in 50 years (Hook, 2011; Xu et al., 2015). It affected more than 60 million people and led to the closure of China's and Asia's largest waterway, Yangtze River, to ships resulting in lost revenue amounting to billions of dollars

1.4. Research objectives and Questions

1.4.1. General Objective

The objective of this research was to improve the understanding of drought variability over the Yangtze River Basin, China from January 2003- Dec 2016 using the standardized drought indices described in section 0, based on remote sensing data and regional water budget in the Jialin-Mintuo sub-catchment.

1.4.2. Specific Objective

- a. **To assess the consistency of the SDI drought indices in describing the same event**
 - Is there consistency? At what scale/time step can drought be monitored?
- b. **To assess the effectiveness of the standardized indices**
 - How effective is the proposed standardized indices framework in providing a uniform descriptor for different aspects of the same event, other indices, and variables?
 - Can the standardized indices effectively monitor meteorological, agricultural and by extension the hydrological drought?

c. To estimate water balance closure using different satellite observations

- What is the sub-catchment annual and monthly water balance closure?
- What information does the water balance relay with respect to drought?

2. THEORETICAL BACKGROUND

2.1. Drought

2.1.1. Definition

Drought is a highly variable complex phenomenon caused by sustained below-average areal precipitation. It is a function of meteorological and climatic influences and interactions such as precipitation, evaporation, snow, humidity, wind and temperature. Drought characteristics; onset, extent, intensity and severity are identified through drought indices. Droughts exhibit significant spatial and temporal variability from one region to another and climate.

2.1.2. Classification

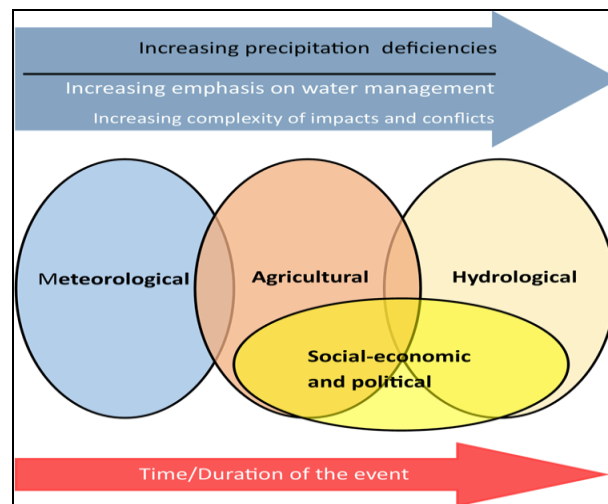


Figure 2-1: Interrelationships between meteorological, agricultural, hydrological and socio-economic drought (Wilhite & Glantz, 1985).

Wilhite & Glantz (1985) reviewed the various forms of drought and categorized it into four; meteorological or climatological, agricultural, hydrological, and socioeconomic drought, as schematically represented in Figure 2-1.

- a. Meteorological drought is a result of a prolonged lack of precipitation and marks drought occurrence and onset.
- b. Agricultural drought (soil moisture drought) and meteorological drought are interlinked; with precipitation shortfall, soil moisture deficit, evapotranspiration, or crop failure as the derivatives. Overall, meteorological influences have consequences on agriculture and by extension, the agricultural drought.
- c. Extended periods without rainfall trigger hydrological drought. It manifests itself as reduced streamflow discharge and falling water level (in reservoirs, lakes, or groundwater). It is damaging; and often cause detrimental societal impacts if not mitigated. It is best described by investigating the regional water cycle budget of a place.

- d. Socioeconomic drought concerns the demand and supply of economic goods and is linked to the other three forms of drought. Extended precipitation deficits affect crop productivity, water supply, hydro-electric power generation and industrial productivity. Demand for goods increases and so does exploitation; resulting in huge socio-economic impacts and conflicts.

2.1.3. Drought origin and propagation

Drought manifestation is a function of complex interplay between natural precipitation deficiencies and excessive evapotranspiration over an area in time. Drought is said to have occurred whenever the expected precipitation falls below normal levels consistently over long periods. Drought is a function of air mass movement on the earth's surface. High-pressure weather systems as result of large-scale anomalies in the global circulation pattern of the atmosphere can be responsible for long-term drought events. For example, winter drought can develop when precipitation is stored as snow and does not contribute to groundwater, soil moisture and streamflow recharge. Climatic factors such as high winds and low humidity intensify drought. Drought occurrence and type is dictated by climate, atmosphere and ocean geographical location, wind patterns and catchment characteristics; with precipitation being the main driver. Reduced groundwater levels and streamflow can indicate and infer drought (Changnon, 1987, as cited in USGS, 2012). However, there exists a time lag before the shortages in precipitation manifest in streamflow and groundwater (Wilhite, Svoboda, & Hayes, 2007).

2.1.4. Indices

Drought indices are numerical representations used to determine drought severity as assessed through climatic and hydrometeorological variables such as temperature, precipitation, streamflow, groundwater and reservoir water levels. Each index is uniquely superior and addresses a specific aspect of the water cycle (Zargar, Sadiq, Naser, & Khan, 2011). The indices quantify drought at varying time-scales (Wilhite et al., 2007), based on four drought distinct characteristics: intensity, onset, severity and duration (Wilhite & Glantz, 1985; Zargar et al., 2011). Severity refers to the departure from normal of an index, often identified by setting a threshold. The onset refers to the start of the period of time when the index starts to fall below the threshold, duration defines how long the drought persist. Monitoring the climate at different timescales enable us to identify and capture both short-term and long-term droughts. Yearly and monthly timescales are often used. However, drought indices are limited to need (study interest), scope and data.

Meteorological drought result from precipitation failure and is assessed through indices that describe precipitation decline, such as the rainfall anomaly index (RAI; van Rooy, 1965) and the SPI (Mckee et al., 1993). SPI is robust and universally preferred. Other indices like the Palmer Drought Severity Index (Palmer, 1965) are also widely used. However, its estimation is laborious. Indices concerned with the rooting zone soil moisture status are include, the SEBS-DSI (Su, 2002), the soil moisture drought index (SMDI; Hollinger et al., 1993), evapotranspiration deficit index (EDI; Narasimhan & Srinivasan, 2005) and the (SPEI: Vicente-Serrano et al., 2010). Agricultural drought describes vegetation changes an include vegetation condition index (VCI; Kogan, 1990).

2.1.5. Standardised drought indices

Standardized indices exist alongside the drought indices discussed in section 2.1.4. For this study, the standardized precipitation index SPI (Mckee et al., 1993), standardized actual evapotranspiration index (SPA EI; Homdee et al., 2016), the standardized vegetation index (SVI, Peters et al., 2002) and the standardized terrestrial water storage index (STWSI) were considered.

2.2. Drought related studies in China

Considerable research has been done to quantify and understand drought patterns and meteoric influences in China especially in the Yangtze River basin /Tibetan plateau. Huang et al. (2013) analysed long-term terrestrial water storage changes in the Yangtze River basin using 32-year (1979-2010) TWS data from ERA-Interim and GLDAS-Noah model validated using 26-year (1979-2004) runoff data from Yichang gauging station and compared to 32-year precipitation data from the GPCC and PREC/L. They reported a significant decline in TWS in the basin since 1998, with 2005-2010 the driest, especially in the middle and lower sections of the river due to decreased precipitation. In a follow-on study, Huang et al. (2015) using GRACE and GLDAS data hydrologically modelled the TWS over the Yangtze River Basin to estimate the effect of human activities on terrestrial water storage from 2003-2010. They found that the TWS was increasing at 3cm p.a. in the middle and lower sections of the basin due to excess artificial recharging of the water stable through large-scale irrigation; following the 2003-2010 drought.

Xu et al. (2015) analysed the spatio-temporal trend of drought in China from 1961-2012 using the 3-month SPI, SPEI and RDI and concluded that the two severest drought events occurred in 1962-1963 and 2010-2011 as a result of decreased precipitation. The drought affected over 50% of non-desert regions too and was severest around North China stretching downstream of the Yangtze River.

Yu et al. (2014) used the SPEI to assess severity and frequency of agricultural drought over China from 1951-2010 and concluded that extreme and severe drought had increased since the late 1990s and was more frequent, severe, and considerably variable across China; with the Northern parts most affected, mainly due to decreased precipitation coupled with general increase in temperature. Yang et al. (2013) studied the characteristics and spatial distribution of droughts in China from 1961-2010 based on Multi-Scale Standardized Precipitation Index (MSPI) and concluded that extreme severe drought events resulted from low precipitation and high ET and were clustered in autumn with areas SW of China experiencing rapid increase. According to Wang et al. (2016), drought in china is a function of the monsoon climate and droughts have increased. Severe drought occurred in southwestern China in 2010 and the middle/lower Yangtze Basin in 2011.

2.3. The standardized drought indices

2.3.1. SPI

The Standardized Precipitation Index (SPI) is the commonest precipitation-dependent drought index requiring precipitation data and is easy to calculate. However, long-term(at least 30 years) precipitation data is needed to accurately characterize drought events (Mckee et al., 1993). SPI standardization uses the gamma probability transformation (Equation 2-1) to normalize the precipitation data before transformation to a standard Gaussian multivariate with a mean of 0 and a standard deviation of 1.

SPI calculation follows three steps (Mckee et al., 1993):

- Precipitation record is converted to a probability density function by applying the Gamma PDF, Eq. 2-1
- Then the resulting PDF is then transformed to a cumulative density function (CDF), using Eq.2-3
- The CDF is then transformed to a standard normalized Gaussian multivariate by applying Gaussian inverse transform. The result is the SPI values. Positive SPI values indicate of wet periods and vice-versa. Consistent values less than zero to -1 or less, indicate drought onset (Mckee et al., 1993)

$$g(x) = \frac{1}{\beta^\alpha \Gamma(\alpha)} x^{\alpha-1} e^{-\frac{x}{\beta}}; \text{ for } x > 0; \alpha > 0; \beta > 0 \quad 2-1$$

Where: α is the shape parameter, β is a scale parameter and x is the precipitation variable and $\Gamma(\alpha)$ is the gamma function defined by Equation 2-2

$$\Gamma(\alpha) = \int_0^x x^{\alpha-1} e^{-x} dx \quad 2-2$$

The cumulative probability density function is defined by the integral of $g(x)$ w.r.t x

$$G(x) = \int_0^x g(x) dx = \frac{1}{\beta^\alpha \Gamma(\alpha)} \int_0^x x^{\alpha-1} e^{-\frac{x}{\beta}} dx \quad 2-3$$

The SPI concept largely borrows from the standardization procedure presented in Equation 2-4 and is basically the number of standard deviations the cumulative precipitation deficit deviates from its normalized long-term average.

$$SPI = \frac{P(i) - \mu(P)}{\sigma(P)} \quad 2-4$$

Where $P(i)$ is the precipitation variable, $\mu(P)$ the long-term/climatic average and $\sigma(P)$ is the climatic standard deviation.

SPI is multi-scalar and assumes that precipitation variability is more pronounced than other meteorological influences like temperature and evapotranspiration (ET), and that all other influences/variables are static and without temporal trend (Vicente-Serrano, Beguería, et al., 2010).

Table 2-1: Classification of SPI values (Mckee et al., 1993)

Category	SPEI
Extremely dry	values Less than -2
Severely dry	-1.99 to -1.5
Moderately dry	-1.49 to -1.0
Near normal	-1.0 to 1.0
Moderately wet	1.0 to 1.49
Severely wet	1.50 to 1.99
Extremely wet	More than 2

2.3.2. SPEI

Like the SPI, the Standardized Precipitation and Evapotranspiration Index (SPEI) is multi-scalar and uses the difference of P and PET (rainfall excess) rather than precipitation alone to estimate drought severity, duration, frequency and intensity. It is adaptable over a wide range of climates; and allows for spatio-temporal comparison of drought events. SPEI extends the SPI and is estimated similarly. The main difference being that it takes into accounts both P and PET data into the calculation ($D=P-PET$) aggregated at various time scales. By incorporating the PET into the estimation, the impact of temperature on water

demand is assessed, and drought severity captured better (Vicente-Serrano et al., 2014). PET is calculated based on the globally accepted Penman-Monteith method (Beguería et al., 2014; Vicente-Serrano et al., 2010). Like the SPI, the SPEI is multiscalar; with calculation timescales ranging from 1-48 months.

The difference between the precipitation (P) and PET for the month represents a simple measure of the water surplus or deficit for the analyzed month. In principle, surplus indicates wetness and deficits indicate drought. The D-series is then fitted to a log-logistic probability distribution to transform the original values to standardized units (Gaussian variate with zero mean and standard deviation of 1) comparable spatially and temporally. The log-logistic PDF is preferred as it fits extreme values better than the three-parameter distributions (Vicente-Serrano et al., 2010). Positive values of SPEI indicate above average moisture conditions while negative values indicate below normal (drier) conditions. The log-logistic probability distribution function of a variable D is defined using Eq. 2-5

$$F(D) = \left[1 + \left(\frac{\alpha}{D - \gamma} \right)^\beta \right]^{-1} \quad 2-5$$

Where α , β and γ are the scale, shape and location parameters estimated from the D (P-ET_a).

The multi-scalar characteristics of the SPEI make it superior to other widely used ET based drought indices used to identify drought type and impact with respect to global warming (Beguería et al., 2014). The SPEI is temporally flexible and spatially consistent and reflects the water deficits at different time scales. It is more suitable to investigate drought characteristics and assess moisture conditions (Potopová et al., 2015).

Table 2-2: The SPEI drought categories.

Category	SPEI
Extreme dryness	values Less than -2
Severe dryness	-1.99 to -1.5
Moderate dryness	-1.49 to -1.0
Near normal	-0.99.0 to 0.99
Moderate wetness	1.0 to 1.49
Severe wetness	1.50 to 1.99
Extreme wetness	More than 2

For this study a different index, the SPAEI (Homdee et al., 2016), premised upon the SPEI is considered. Thus, the SPEI formulation and parameterization details are skipped but can be found in (Vicente-Serrano et al., 2010).

2.3.3. SPAEI

The Standardized Precipitation and Actual Evapotranspiration Index SPAEI (Homdee et al., 2016) formulation and calculation is similar to that of SPEI. The key difference is that the PET is substituted with actual evapotranspiration (ET_a) in calculating the water deficits and the Generalized Extreme Values (GEV) probability distribution rather than the log-logistic PDF used to normalize the deficits (P-ET_a). Like the SPEI and SPI it is multiscalar; aggregated at 1, 3, 6, 9, 12, 24-months or longer and uses the same drought classification as the SPEI shown in Table 2-2. The SPAEI follows Stagge et al. (2015; 2016) review on SPEI (Vicente-Serrano et al., 2010) methodology and recommendation that the GEV is superior to the log-logistic

PDF currently used to normalize the P-PET series. Stagge et al. (2015; 2016) evaluated the performance of the log-logistic PDF against other PDF's: the GEV, log-normal and the Pearson Type III distributions and concluded that based on the Shapiro-Wilk and the Kolmogorov-Smirnov (K-S) goodness of fit tests, unlike the log-logistic PDF that is invalid and undefined when the D series is negative, the GEV is unbounded, simulates the extremes adequately and had the best goodness of fit across all timescales. Based on Stagge et al. (2016) re-assertion that the GEV is superior to log-logistic distribution, the GEV was thus adopted.

The Generalized Extreme Value (GEV) distribution is a flexible three-parameter distribution that combines the Gumbel (Type-I), Fréchet (Type-II), and Weibull (Type-III) maximum extreme value distributions to fit the probabilities of sporadic and stochastic variables. The GEV PDF is defined by Eq. 2-6.

$$f(x) = \begin{cases} \frac{1}{\sigma} \exp(-(1+kz)^{-1/k}) (1+kz)^{-1-1/k} & k \neq 0 \\ \frac{1}{\sigma} \exp(-z - \exp(-z)) & k = 0 \end{cases} \quad 2-6$$

Where $z = \frac{(x-\mu)}{\sigma}$, and k, σ , μ are the shape, scale, and location parameters respectively. The scale must be positive, i.e. ($\sigma > 0$), the shape and location parameters are real values. The GEV distribution domain depends on k defined by Equation 2-10:

$$\begin{aligned} 1 + k \frac{(x-\mu)}{\sigma} > 0 & \quad \text{for } k \neq 0 \\ -\infty < x < +\infty & \quad \text{for } k = 0 \end{aligned} \quad 2-7$$

The cumulative distribution function, CDF is defined by Equation 2-11

$$F(x) = \begin{cases} \exp(-(1+kz)^{-1/k}) & k \neq 0 \\ \exp(-\exp(-z)) & k = 0 \end{cases} \quad 2-8$$

The GEV functionality is available in MATLAB. The SPAEI has only been applied in Thailand and this is the second research the SPAEI is used. The novelty in this research is that the SPAEI is used in combination with other standardized drought indices for the first time over China.

2.3.4. SDSI-ETDI

The standardized drought severity index-evapotranspiration deficit index is a combination two drought indices: the DSI (Su et al., 2003; developed to infer rooting zone soil moisture from SEBS) and the ETDA (Narasimhan & Srinivasan, 2005; used to simulate water stress anomalies based on ETa and PET). The SDSI-ETDI is the standardized combination of the two and is useful in identifying crop water stress based on surface energy balance estimates.

Temporal changes of the ET as a function of the soil moisture water content are tracked as the only fraction of the water being evaporated from the earth's surface in absence of precipitation or irrigation. The concept assumes that the fluxes occur within the soil matrix in a vertical direction, upon which the volumetric soil moisture changes are then estimated, and parameterized from first principles of mass conservation, as a direct relation of the relative soil moisture to ET; defined as the relative soil moisture deficit in the root zone i.e. $D=1-R$ where R is the evaporative fraction (Su, 2002). DSI is high when SM is low and vice versa.

ETDI follows a similar approach to quantify the water stress ration i.e. $(WS=(ET_0-ET)/ET_0)$; where ET_0 is the weekly/monthly reference evapotranspiration, and ET is the actual weekly/monthly ET . Adopting a similar standardization procedure to that of SPI (Equation 2-4) the water stress ratio is then compared to the median calculated over a long-term period and hence the SDSI-ETDI. Values less than zero indicate water stress/drought and vice versa. ETDI is useful in estimating the onset, duration, and intensity of drought.

The study envisaged to use SM data to calculate the SDSI-ETDI. Soil moisture data was obtained from GLDAS for the period January 2002 to November 2017. ETDA is calculated from a combination of ET , PET or the $NDVI$. However, calibrated PET measurements over China and study period were unavailable. The global FEWSNET PET was explored. However, available data is inadequate (spans 2002 to March 2014). Also, due to time constraint, the SDSI-ETDI was therefore not considered.

2.3.5. SVI

The standardized vegetation index (Peters et al., 2002) provides a basis to quantify and assess drought by standardizing the $NDVI$ ^{2.9} to describe the probability of the vegetation condition based on $NDVI$ deviations from the normal on a weekly/monthly scale. The probability of drought occurrence is determined using z-scores of the $NDVI$ (greenness) distribution with respect to the historical vegetation condition at a given location. The Z-score is a deviation from the mean in units of the standard deviation, calculated from the $NDVI$ values for each pixel location for each week for each year for the period of observation using Equation 2-10.

$$NDVI = \frac{\rho_{NIR} - \rho_R}{\rho_{NIR} + \rho_R} \tag{2-9}$$

$$Z_{xy,t} = \frac{NDVI_{xy,t} - \overline{NDVI_{xy}}}{\sigma(xy)} ; SVI = P(Z < Z_{xy,t}) \tag{2-10}$$

The $NDVI$ is calculated on a per-pixel basis as the normalized difference between the red and near infrared reflectance bands of a satellite image. Where $Z_{xy,t}$ is the pixel z-value over time time (t), $NDVI_{xy,t}$ is the weekly/monthly pixel-pixel $NDVI$ value over time, $\overline{NDVI_{xy}}$ is the pixel mean $NDVI$ for pixel σ the standard deviation of the $NDVI$.

The Z-scores are assumed to be normally distributed with a mean of zero and standard deviation =1 (Peters et al., 2002). The Z-scores are then converted to probabilities ranging between 0 and 1, corresponding to very poor-very good as shown in Table 2-3. It is good for investigating vegetation response to short-term weather conditions and useful as a near-real-time indicator of onset, extent, intensity, and duration of vegetation stress in areas of varying drought conditions. However, it is affected by crop phenology and blooms.

Table 2-3: The SVI drought classification (based on probability of occurrence)

Category	SVI
Severe drought	0 - 0.10
Moderate drought	0.10 - 0.25
Slight drought	0.25 - 0.5
Normal	0.5 - 0.75
Favourable	0.75 - 1

2.3.6. STWSI

The terrestrial water storage (TWS) is a function of the all the water cycle components and phases of water stored above and below the Earth's surface including soil moisture, snow and ice, canopy water storage, groundwater among others. TWS influences earth's energy, water, and biogeochemical fluxes. The fluxes are monitored by the GRACE satellite, launched in March 2002 and operated *NASA*' Jet Propulsion Laboratories (JPL). Changes Earth's gravity field is picked as the TWS and can be inferred on a monthly scale. The GRACE satellite was launched in to provide information on Earth's TWS.

The standardized terrestrial water storage index (STWSI) followed a similar standardization approach using Eq. 2-11

$$.STSWI_{ijk} = \frac{TWSI_{ijk} - \overline{TWSI}_{ij}}{\sigma(ij)} \quad 2-11$$

Table 2-4: The STWSI drought classification

Category	STWSI
Extreme dryness	values Less than -2
Severe dryness	-1.99 to -1.5
Moderate dryness	-1.49 to -1.0
Near normal	-0.99.0 to 0.99
Moderate wetness	1.0 to 1.49
Severe wetness	1.50 to 1.99
Extreme wetness	More than 2

3. STUDY AREA AND DATA

3.1. Study area

Yangtze River is 6300km long and is the longest river in China and Asia, and the third longest river in the world after the Nile and the Amazon. It has sources in the Qinghai-Tibetan Plateau high altitudes (Geladaindong Peak) and flows eastwards to enter the sea at East China Sea, near Shanghai. Geographically, it lies between 24°30'-35°45'N and 90°33'-120°55'E. The river's mean annual discharge is approximately 32000m³/s.

The Yangtze River Basin spans 1.8Mkm² and is an important lifeline that sustains half of China's population. It accounts for more than 40% fresh water resources in China and more than 70% grain-produce. The 37km iconic Three Gorges Dam is located here and is also home to major cities like Shanghai, Nanjing and Chengdu. The Cuntan gauging station (106.568°E, 29.571°N) is the entrance to the Three Gorges Dam (S. L. Yang et al., 2010).

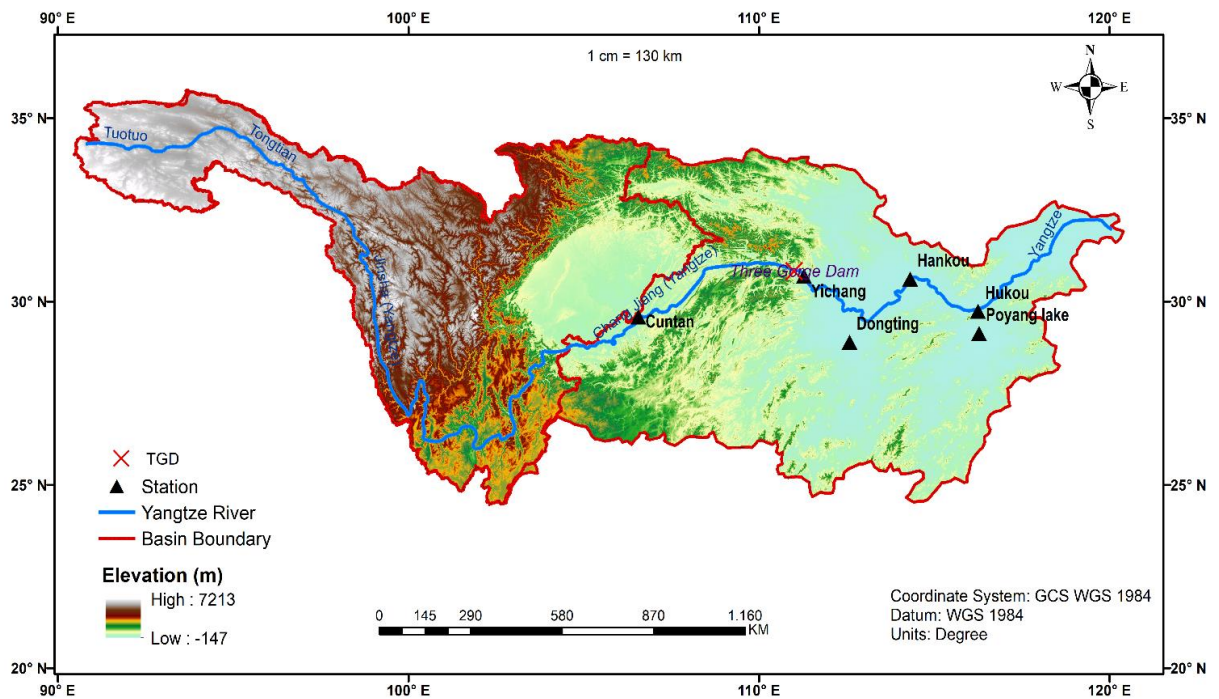


Figure 3-1: Study area

3.1.1. Physiography

The Yangtze River Basin has three distinct geographically-influenced morphological zones: the Qinghai-Tibet plateau, middle-range Mountains, and the eastern lower plains; corresponding to the upper, middle and the lower reaches respectively. Rapids and shoals are characteristic in the upper reaches spanning from the westernmost point Tatouhou to Yichang (90.6°E and 104.3°E). The middle section spans from Yichang to Hukou in Jiangxi Province (104.3–111°E), and the lower reaches extends from Hukou to the river mouth

near Shanghai (111–121.8°E) as shown in Figure 3-1. Mean altitude graduates from 3720m a.s.l. in the upper reaches, 1560 m a.s.l. in the middle section to 400m a.s.l in the lower section.

3.1.2. Climate

Precipitation

The Yangtze basin lies in the subtropical monsoon climatic belt bordering the tropical climate to the south and temperate climate to the north. Climatic mean annual precipitation of the basin is 1067mm although it varies spatially (Huang et al., 2015; Q. Zhang, Jiang, Gemmer, & Becker, 2005). The variability is a function of the tropical monsoon influences, tidal changes in the Inter-Tropical Convergence Zone (ITCZ) and topography.

Except for some areas within the Tibet plateau, most parts of the Yangtze basin experiences subtropical-monsoon climate characterized by quad-modal season transitions: winter, summer, spring and autumn. Winter runs from December through February, spring from March to May, summer from June to August and autumn from September to November. The rainfall pattern is influenced two yearly monsoon air flows: the Siberian northwest winter monsoon and the Asian southeast summer monsoon (or Indian southwest summer monsoon on the upper Yangtze reaches) (Zhai, et al., 2005). Precipitation is heaviest in summer, with July the wettest and warmest. Winter season is mostly dry. January is the driest and coldest. Western parts of the basin are drier than the eastern parts. Basin mean annual precipitation varies from 300-500mm in the western region to 1,600-1,900mm in the south-eastern region (Q. Zhang et al., 2005).

Temperature

The temperature patterns over the Yangtze Basin vary from place to place as influenced by relief (topography) and the monsoon. Temperatures are lowest in January (winter) and highest in July (summer). Mean monthly temperature ranges from -5°C in January to 16°C in July. The mean annual air temperature ranges from -4.5°C on the Tibetan Plateau to 21.3°C to the southern edge of the basin (Sun, Miao, & Duan, 2015). Northern regions are warmer than the southern regions.

3.2. Data

In the study, both in-situ and remote sensing data are used at various temporal and spatial characteristics as summarized in Table 3-1.

Table 3-1 Datasets characteristics and source

Data	Source	Characteristics
Precipitation (P)	CHIRPS quasi-global precipitation product	Monthly precipitation gauge-satellite based precipitation at $0.05^{\circ} \times 0.05^{\circ}$ from Jan 1981-Aug 2017 downloaded from CHIRPS website http://chg.geog.ucsb.edu/data/chirps/ in netCDF.
Evapotranspiration (ET)	SEBS	Monthly ET measurements spanning Apr 2000 to July 2017 estimated using the revised SEBS algorithm (X. Chen et al., 2014) at $0.05^{\circ} \times 0.05^{\circ}$ spatial scale. Downloaded from the Third Pole Environment Database website: http://en.tpdatabase.cn/portal/MetaDataInfo.jsp?MetaDataId=249454
Discharge (RO)	In-situ	Monthly flow measurements (m^3/s) spanning 2005-2010 obtained from Cuntan gauging station on R. Yangtze
Terrestrial Water Storage	GRACE Tellus satellite	Monthly terrestrial water storage measurements measured by the GRACE-Tellus satellite land water products spanning Apr 2002 to Jan 2017 at $1^{\circ} \times 1^{\circ}$ spatial scale downloaded from ftp://podaac-ftp.jpl.nasa.gov/allData/tellus/L3/land_mass/RL05/netcdf/ and was interpolated to $0.05^{\circ} \times 0.05^{\circ}$ grid scale.
Modis Vegetation Indices data (MOD13C2.005)	USGS Land Processes Distributed Active Center (LP DAAC) dataset discovery portal	Version 6 MODIS/Terra Monthly vegetation indices L3 Global at 0.05° spatial scale spanning Feb 2000- Aug 2017. Downloaded from the USGS portal. https://lpdaac.usgs.gov/dataset_discovery/modis/modis_products_table

3.2.1. Discharge measurements

In-situ monthly discharge (R) measurements taken from the Cuntan gauging station on the Yangtze River from 2005-2010 were used to check agreement in the basin water balance runoff estimated using satellite products, P, ET and TWS, and by extension, the hydrological drought by comparing streamflow regimes over time.

3.2.2. Precipitation

CHIRPS Global rainfall product developed by the USGS and the Climate Hazard Group at the University of California, Santa Barbara is used. It is a quasi-global rainfall product spanning $50^{\circ}N/S$, covering all longitudes. CHIRPS employ the modified distance weighting method algorithm to incorporate satellite information built around a 0.05° climatology data (CHPclim), to represent sparsely gauged locations. Rainfall estimates are derived from thermal infra-red cold cloud duration (CCD) estimates calibrated with global monthly climatology precipitation (CHPclim) at 0.05° , estimated from FAO and Global Historical Climate Network (GHCN) gauge data. (Funk et al., 2015). It is available at daily, pentad or monthly epochs.

The higher spatial resolution (0.05°) coverage and a rich historical database spanning 30+ years (from 1981) makes it superior and useful for trend analysis and seasonal drought monitoring (Funk et al., 2015). Here, the 0.05° monthly global CHIRPS product is used. Data source and characteristics are summarized in Table 3-1.

3.2.3. Evapotranspiration (SEBS ET)

The surface energy balance system, SEBS model, (Su, 2002) approximates the surface energy balance, evaporative fraction, and evapotranspiration based on radiometric data combined with in-situ meteorological data (Peng, Loew, Chen, Ma, & Su, 2016; Su, 2002). It is a single-source energy balance algorithm that initially estimates the sensible heat flux (H) based on the Monin-Obukhov theory with the surface temperature, the aerodynamic resistance and air temperature gradient as inputs.

Sensible heat flux (H) is constrained within two boundaries, the upper and the lower boundary using the dry and wet limiting conditions. H is maximum under the dry limit when ET is zero. Conversely, ET is maximum when sensible heat (H) is lowest, i.e. the wet limit. ET is estimated by establishing energy balance closure against the net radiation, the calculated H and ground heat fluxes. Application of SEBS does not require a priori knowledge of the actual turbulent heat fluxes thus is independent. It is accurate to 20-25% mean error (Su, 2002).

Readymade satellite ET products are available and downloadable at different spatial and temporal resolutions nowadays (Chen et al., 2014; Peng et al., 2016) For this study 0.05° spatial resolution and monthly temporal resolution is required to match other selected products. Processed and calibrated 0.05° global monthly evapotranspiration (mm d^{-1}) estimated using the updated SEBS algorithm (Chen et al., 2014) spanning April 2000 to June 2017 was used.

The global ET product was subset to the region covering China's Yangtze basin ($90-120.5^\circ\text{E}$ and $24-35.55^\circ\text{N}$) in MATLAB and used to calculate the SPAEI and to estimate the water balance trend. Data source and characteristics are summarized in Table 3-1.

3.2.4. MODIS NDVI

Moderate Resolution Imaging Spectroradiometer (MODIS) sensor is onboard NASA's polar-orbiting EO satellites Terra and Aqua launched on December 18, 1999, and on May 4, 2002 respectively. The spacecraft orbit the earth from north to south inclined at 98° and ascend across the equator at the same local time; in the morning for Terra and afternoon for Aqua (Maccherone, 2014). The MODIS satellite characteristics include: wide viewing swath (2330km), 1-2day temporal resolution and varied spatial resolution at 250m (band1 and 2), 500m (band3 to band7) and 1km. The blue, red and NIR reflectance bands are centered at 469nm, 645nm and 858nm respectively.

MODIS processed products range from ocean to land EO data. The NDVI product considered here is the level-3 validated monthly Vegetation Index product (L3 Global MOD13C2.006) projected to 0.05° geographic Climate Modelling Grid (Maccherone, 2014); downloaded from the MODIS website as detailed in Table 3-1.

The NDVI product is derived from cloud-free spatial composites from the 16-day 1-km gridded MOD13C2A2 product; retrieved from daily, atmospherically-corrected, bidirectional surface reflectance (Maccherone, 2014). The 0.05° monthly MODIS NDVI (MOD13C2.006) was used to calculate the SVI and by extension, map the agricultural drought.

3.2.5. GRACE

The GRACE mission uses two synchronized space crafts (Tom and Jerry) 200 km apart to orbit the Earth at an altitude of 500 km to measure time variations of the Earth's gravity field by continuously measuring the distance between the two satellites. Inference on the terrestrial water and ice-sheet movement is then made from the anomalies in the local pull of gravity as water shifts around the earth due to seasonal and climatic fluctuations. Since launch in March 2002, it has been pivotal in providing information on terrestrial water changes using the highly precise K-band microwave system (Tapley, Bettadpur, Watkins, & Reigber, 2004).

Initially programmed for an eight-year expedition, GRACE exploration program is in the extended phase; at a cost. Atmospheric drag on the satellites has decayed the satellite's orbit to about 350km (Long, Longuevergne, & Scanlon, 2015). The batteries cells aboard GRACE too are failing; with a consequent that data is not collected when the satellite is eclipsed. Thus, available data is intermittent; missing several records in some years.

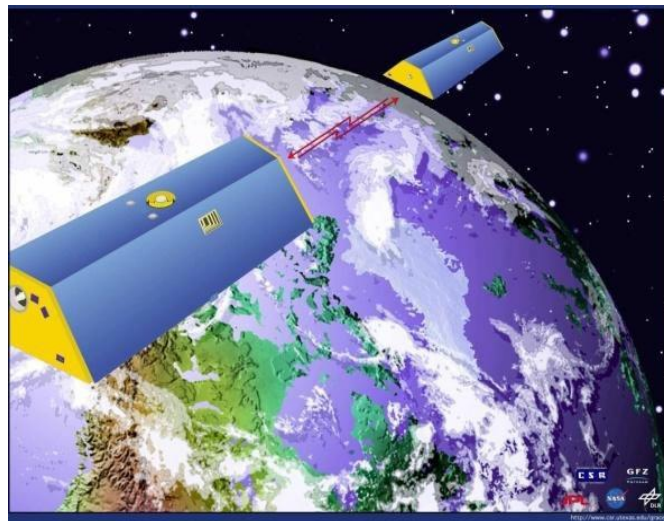


Figure 3-2: The GRACE twin satellites orbiting the earth at an altitude of 500 km and at 220 km distance apart. (University of Texas Center for Space Research).

Terrestrial Water Storage (TWS) is the total amount of water stored on the earth's surface and subsurface and includes soil moisture and permafrost, snow and ice, and wet biomass (Richey et al., 2015). It is a fundamental component of the global hydrological cycle that influences the water, energy and biochemical fluxes and the earth's climate by extension (Jiang et al., 2014; Rodell & Famiglietti, 2001).

For this study, the monthly GRACE Tellus Terrestrial Water Storage (TWS) anomalies (cm) data; calculated as deviations from the mean value for the period 2002 to 2017 at $1^\circ \times 1^\circ$ is used. The product is readymade pre-processed by Sean Swenson and supported by the *NASA MEASURES Program*². The data is derived from spherical harmonic data with order and degree up to 60. These are smoothed by the half-width equivalent to 300km of Gaussian smoothing radius. Figure 3-3 shows the global TWS estimate from GRACE satellite for April 2003.

² <https://grace.jpl.nasa.gov/data/get-data/monthly-mass-grids-land/>

Jiang et al. (2014) reviewed how GRACE data can be used to monitor terrestrial hydrology at large scale and documented three categories: TWS changes monitoring, hydrological components evaluation, and drought analysis and glacier mass balance detection. They cite Leblanc et al. (2009) work who studied multi-year drought evolution in southeast Australia using GRACE TWS from 2001-2008 and found a high correlation between GRACE TWS and the total water deficits at the basin scale.

The GRACE TWS product is used to determine the STWSI and estimate the water balance agreement. It was downloaded, processed, and downscaled to 0.05° in MATLAB. The downscaling procedure and results is covered in GRACE data.

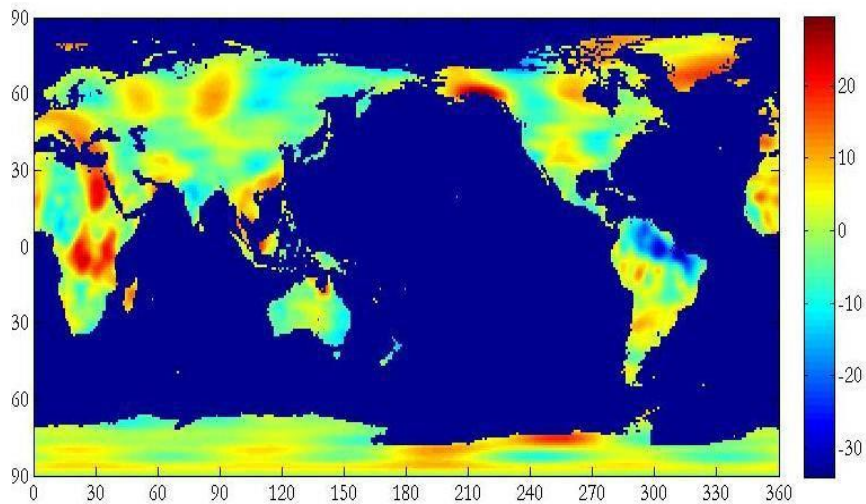


Figure 3-3: GRACE level 3 data of Terrestrial water storage for April 2003.

4. METHODOLOGY

Figure 4-1 summarizes the conceptual research methodology adopted. Figure 4-2 details dataset utilization and role in the research.

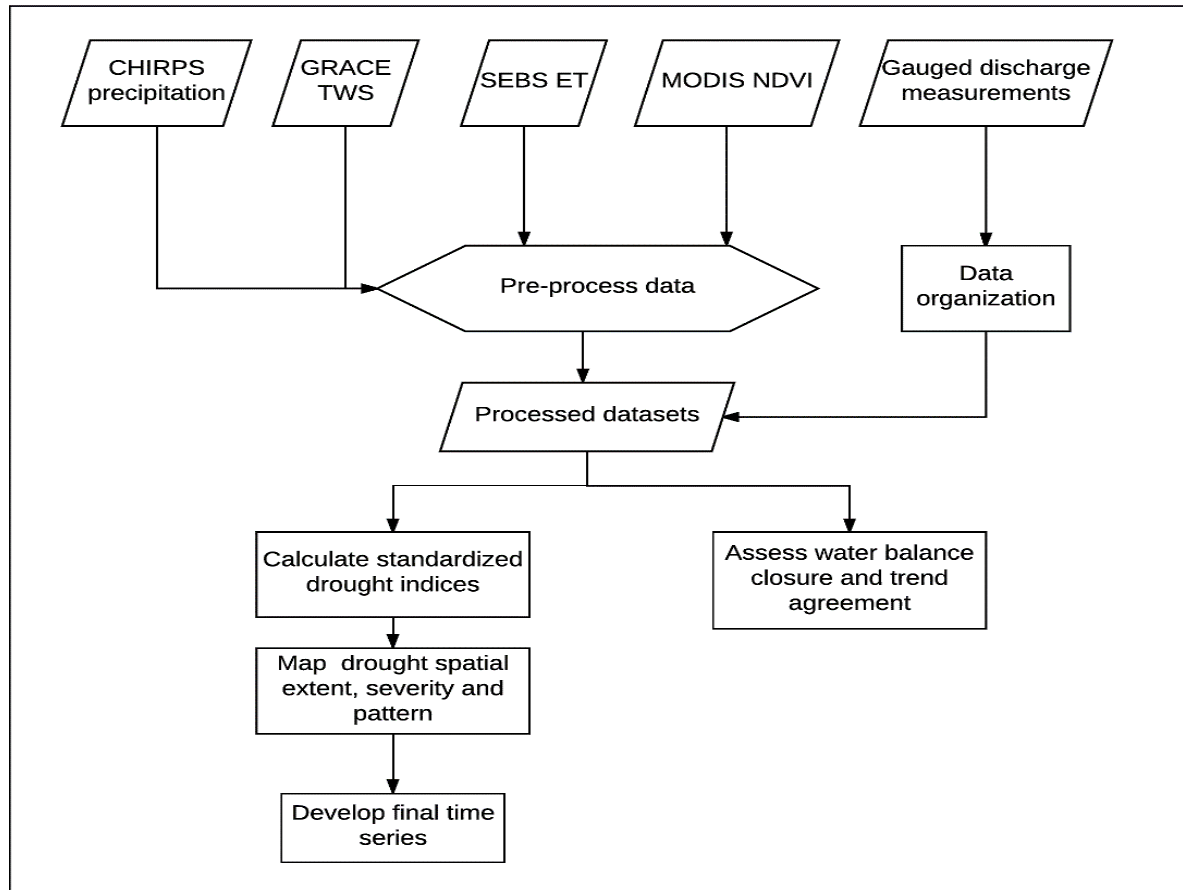


Figure 4-1: Methodology

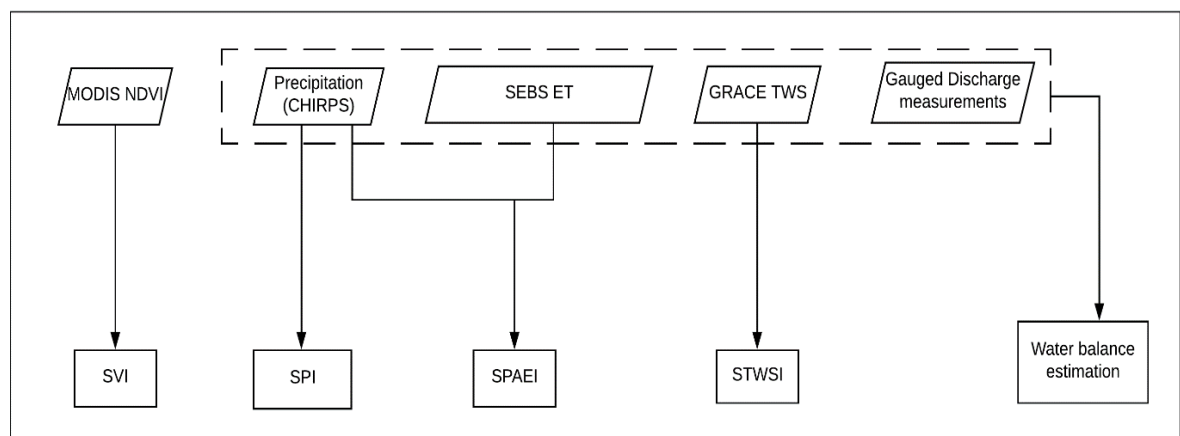


Figure 4-2: Datasets used to calculate the indices and estimate water balance

4.1. Data processing

Data pre- and post-processing was done in MATLAB version 2017b although ILWIS and ArcMap 10.5 among other desktop GIS and remote sensing data processing applications were also used in conjunction. Raw data was considered more appropriate to represent natural drought extremes rather than gap-filled data. Thus, apart from cleaning spurious data, data was used as is and no gap-filling or secondary processing was done. Nevertheless, GRACE data was restructured to include missing months to enable month-month comparison.

4.1.1. MODIS NDVI

Monthly MODIS NDVI product, MOD13C2.006, spanning February 2002 to October 2017 was downloaded and post-processed online using NASA's *LAADS Web interface*². Post-processing parameters included:

- Subset by geographic area of interest to cover the globe
- Reformatting and converting the products to GeoTIFF format and
- Projection to the Geographic map projection, resampling to Nearest-neighbour at $0.05^\circ \times 0.05^\circ$ output pixel size.

4.1.2. GRACE data

The GRACE data netCDF file containing the GRACE Tellus data was downloaded from the GRACE resource centre Table 3-1 and analysed for anomalies. The TWS is the hydrological product available as liquid water equivalent height (LWE) in centimetres at $1^\circ \times 1^\circ$ spatial resolution. A 300km multiplicative Gaussian filter was applied to the LWE to smoothen, normalize and remove correlated errors in GRACE products (Deng, Li, & Song, 2016; Swenson & Wahr, 2006).

Figure 4-3 shows the empirical CDF before and after applying the Gaussian filter.

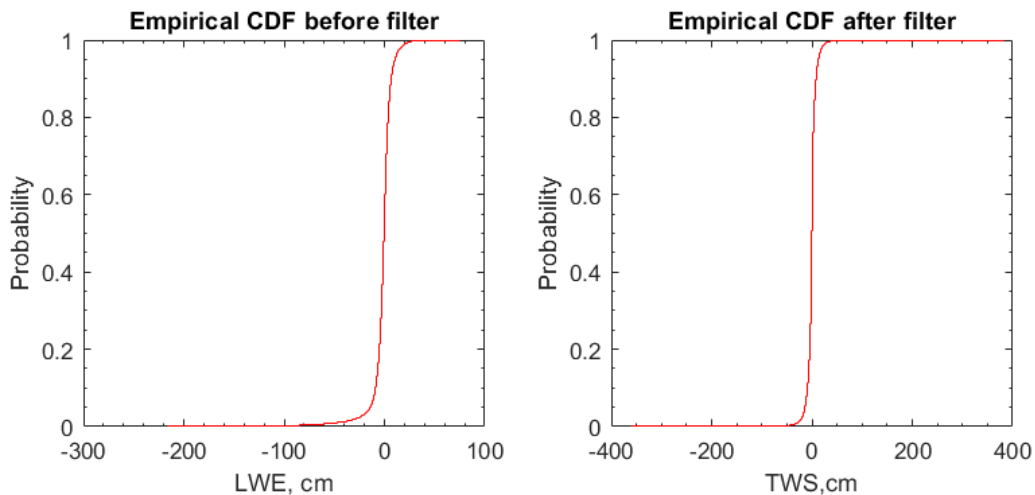


Figure 4-3: Empirical CDF before and after applying the Gaussian filter.

The product was then resampled to 0.05° using bilinear spatial interpolation method using the 2-D gridded interpolation (`interp2`) function in MATLAB shown by Equation 4-1.

$$TWS = \text{interp2}(\text{latg}, \text{long}, \text{LWE}, \text{latp2}, \text{lonp2}, 'bilinear');$$

4-1

Where TWS is the terrestrial water storage (mm), long and latg are the global longitude and latitude mesh-grid at 1° and lonp2, and latp2 is new mesh-grid at 0.05° spatial resolution. LWE is the liquid water equivalent at $1^\circ \times 1^\circ$. Figure 4-4 shows the TWS before and after interpolation.

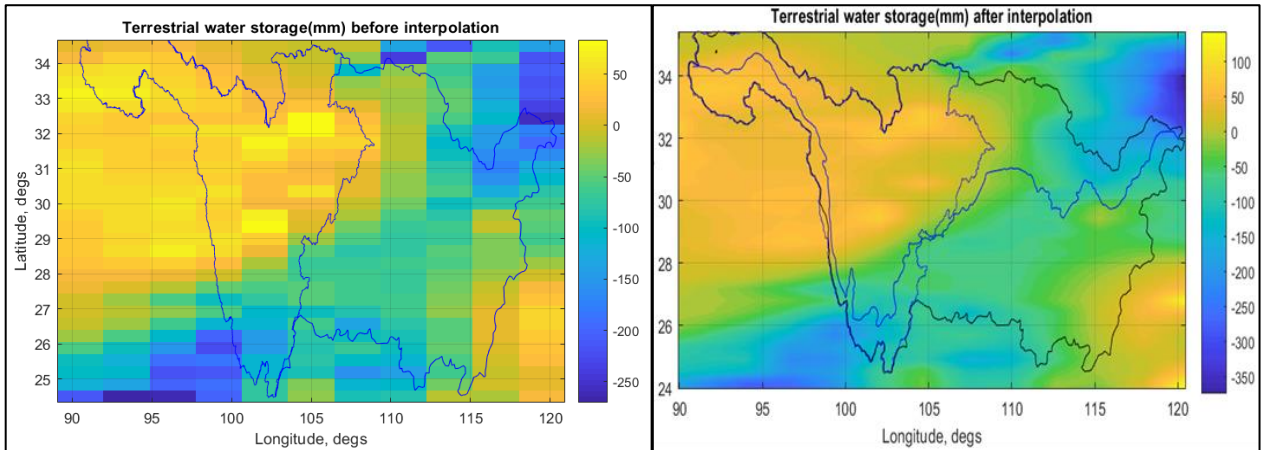


Figure 4-4: TWS before and after spatial interpolation

4.1.3. CHIRPS precipitation

CHIRPS rainfall product was used to calculate the SPI and SPAEI. First, completeness and continuity of the rainfall product were tested. For this, precipitation time series plots were used; to visualize the data and provide ad hoc data quality control (Figure 4-5). Overall, the rainfall record had minimal gaps, exhibited good data quality and was considered reliable. Over the selected pixels, the series exhibit seasonal pattern with mean monthly average rainfall ranging from 700-1100mm. There were no instances of negative rainfall. Monthly precipitation was an input to the multiscale SPI and SPAEI calculation. The moving average function in MATLAB was used to scale the precipitation data at 3, 6, 9, 12 and 24-month intervals running from January 1981-August 2017. The SPI script used for this is included in Appendix 3.

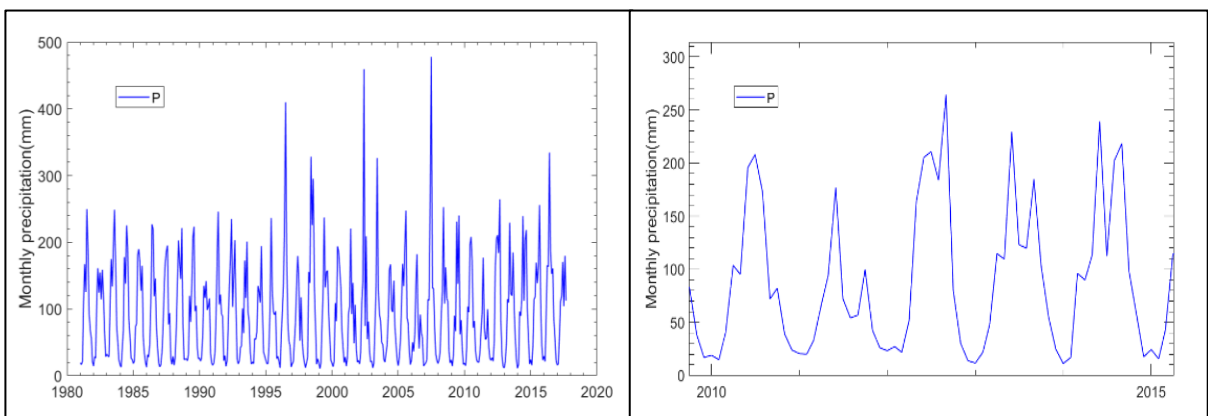


Figure 4-5: Cuntan station precipitation time series, 1981-2017

² <https://ladsweb.modaps.eosdis.nasa.gov/search/order/5/MOD13C2-6/2008-11-02..2017-11-17/DB/World>

4.1.4. Discharge

In-situ discharge measurements obtained from Cuntan Gauging Station were used to assess the overall accuracy of runoff estimated from the satellite products by solving the water balance within the Jialin-Mintuo-Jianshi sub-catchment, in the upper reaches of the River Yangtze Basin () as described in section 4.5.

4.2. Standardised Drought Indices Calculation

The study sought to compare the effectiveness and applicability of the SPI, SPAEI, SVI, and the STWSI to monitor drought. Common statistical drought indices comparison techniques are used to evaluate the performance as discussed.

4.2.1. SPI

McKee et al. (1993) describe the procedure to calculate the SPI as described in section 2.3.1 at depth. As a recap, to calculate the SPI the climatic precipitation record was first fitted to a gamma probability function before transformation to a normal distribution with a mean 0 and a standard deviation of 1 by applying the Gaussian (inverse-normal) function. The result is the SPI, in the range of ± 2.0 , with extremes outside this range occurring at 5% of the time (McKee et al., 1993).

The gamma PDF is preferred to represent variations in precipitation for its flexibility and ability to represent various distributions based on only two parameters, shape(alpha) and scale (beta) (Funk et al., 2015; Husak, Michaelsen, & Funk, 2007; McKee et al., 1993; Wilks, 1990). Additionally, it has an advantage over other PDF in that for it is constrained to zero on the left, it intrinsically filters negative instances as rainfall can never be negative (Husak et al., 2007; Wilks, 1990). It's therefore useful over arid areas and areas characteristic of low rainfall regimes experienced over the Yangtze River Basin. The SPI is multiscalar. To properly characterize drought with the SPI, the CHIRPS precipitation record was scaled at 1, 3, 6, 12, and 24-months moving averages and a gamma probability distribution applied to define the probability relationship.

4.2.2. SPAEI

SPAEI (Homdee et al., 2016) formulation and calculation follow a similar approach to that of SPEI. For the SPAEI, the D_i values-the difference between precipitation and ET_a , are aggregated at 1, 3, 6, 9, 12 and 24-months moving averages and fit to a Generalized Extreme Values (GEV) probability distribution before transformation to the standard normal distribution. The complete procedure for SPAEI calculation is discussed in section 2.3.2. After calculation, trends and magnitudes of the SPAEI are compared and discussed.

4.2.3. SVI

The SVI followed the Z-Score standardization procedure (Equation 2-4) and was calculated by subtracting the long-term mean from pixel value NDVI and then dividing the difference by the standard deviation. The Z-score does not require prior fitting to a probability distribution as it is assumed normally distributed. A consequence of is that the Z-score is believed may not adequately capture drought at shorter timescales especially at 1-month. MODIS Terra NDVI product from 2000-2017 was used to calculate the SVI as explained in section 2.1.5. The MODIS product was pre-processed online on the *NASA* site as explained in section 3.2.4 and was rescaled to NDVI values ranging from -0.2 to +1 by multiplying with a scaling factor, 0.0001, to correct for image distortion and normalized to a mean of 0 and standard deviation of 1.

4.2.4. STWSI

GRACE TWS data was used to calculate the standardized terrestrial water storage index using the standardization method explained in section 2.1.4. As explained in section 3.2.5, the TWS data is discrete and has many gaps occasioned by missing months when no data is transmitted whenever the satellite is eclipsed from the sun. The months in which these gaps occurred were not considered.

4.3. Time series, scatterplot and the qq-plots

The quantile-quantile plot (qq-plot) were used to explore the data and graphically assess how closely a data set fits a distribution. Time series plots were used to present the statistical trends, seasonality/pattern, and multi-year changes. Map-series captured spatial and temporal variation and evolution on maps. Scatter plots and correlation were used to establish the relationship and covariation of the drought indices time series data for the basin and at Cuntan gauging station extracted for the periods January 2003-Dec 2016.

4.4. Statistical Analysis

Regression analysis was done to establish how the indices correlate and at what timescale. This was achieved by determining the r-Pearson coefficients for all the timescales. Pearson correlation coefficient (r), is a dimensionless data-distribution-dependent parametric correlation test used to establish the linear dependence between two normally distributed continuous variables (x and y) (Helsel & Hirsch, 1995; Hennemuth et al., 2013) The plot of $y = f(x)$ is the linear regression curve.

$$r_{Pearson} = \frac{\sum_{i=1}^n (x - \bar{x})(y - \bar{y})}{\sqrt{\sum_{i=1}^n (x - \bar{x})^2} \cdot \sqrt{\sum_{i=1}^n (y - \bar{y})^2}} \quad 4-2$$

Where n =sample size, \bar{x} =arithmetic mean of $x(i)$ and \bar{y} =arithmetic mean of $y(i)$.

The goodness of relationship was assessed using Pearson's regression coefficient (r) calculated using 4-2. r ranges between ± 1 . Data is positively correlated when r is positive and vice versa. A complete positive linear relation is indicated by $r=1$; no relation by $r=0$; and complete negative linear relation by $r=-1$. Regression analysis is widely accepted as basis of drought indices evaluation and has been used by several researchers like (Suliman, et al., 2015).

4.5. Water Balance Estimation

Dynamics of water flow at regional and catchment scale is influenced by many factors such as precipitation, geology, catchment characteristics, soils etc. The fluxes and flow dynamics are best characterized using the water balance estimation approach in order establish the status and trends of water resources in an area over time. In principle, the water balance is defined by the law of conservation of mass as applied to the hydrologic cycle as shown in equation 4-3.

$$\frac{\Delta S}{time} = P - ET - R \quad 4-3$$

Where P is the precipitation (rainfall), E the evapotranspiration, R the discharge and ΔS the change in water storage within the basin over time.

For this study, the catchment upstream the Cuntan gauging station, comprising Jinsha, Mintuo, and Jialing sub-catchments within the upper reaches of the Yangtze River Basin as shown in was considered. It was assumed to be a closed system with a decoupled groundwater component. The only discharge being through

the basin outlet at Cuntan gauging station. However, the assumption may be wrong and may account for closure gaps.

The regional accuracy of the basin runoff estimated using satellite products P (CHIRPS), ET (SEBS) and TWS (GRACE) is assessed against spatially-averaged time series produced using observed discharge measurements ($\text{m}^3\text{s}^{-1}\text{month}^{-1}$) from Cuntan Gauging station for the period January 2005-Dec 2010. Satellite estimates are monthly, in millimetres (mm). The $R(\text{obs})$ time series was averaged spatially based on Balsamo et al. (2009) as cited in (Huang et al., 2015). First, the monthly discharge data was divided by the area of the study area. The satellite pixel-pixel $R(\text{obs})$ estimates are accumulated over the entire area over the study period. The spatially averaged time series of the satellite estimates were then calculated as the spatial mean of the accumulated monthly values of all the pixels within the study area.

The percent bias (PBIAS) objective function was used to assess the systematic bias of the runoff. accuracy and closure as described in Moriasi et al. (2007) calculated with equation 4-4. Where $R(\text{cal})$ is the calculated runoff and $R(\text{obs})$ is the observed discharge.

$$PBIAS = \left(\frac{\sum(R_{cal} - R_{obs})}{\sum(R_{obs})} \right) * 100 \quad 4-4$$

The optimum value for PBIAS is 0, and the closer to zero the bias is, the higher the accuracy. Positive values indicate underestimation, and negative values indicate overestimation.

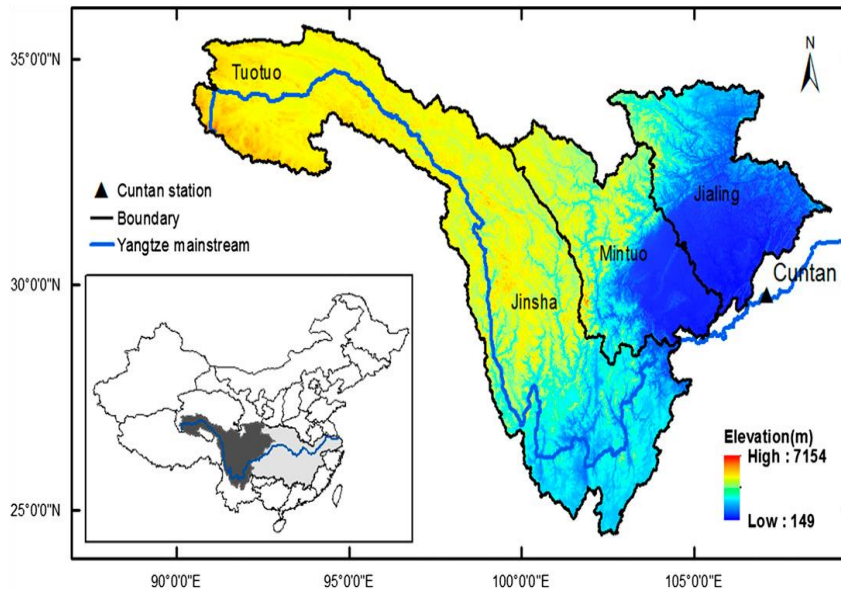


Figure 4-6: Elevation map of the Jinsha, Mintuo, and Jialing sub-basins located in the upper reaches of the Yangtze (Huang et al., 2015)

5. RESULTS AND DISCUSSION

The results of various processes applied to meet the study objectives are presented in this chapter. The results are also discussed in line with selected literature and global practice.

5.1. Precipitation, ET, TWS, SM and NDVI pattern

To understand the behavior of meteorological influences in the Yangtze River basin, spatial averages of the basin mean-monthly and the mean-annual monthly patterns were determined and are shown in Figure 5-1 and Figure 5-2.

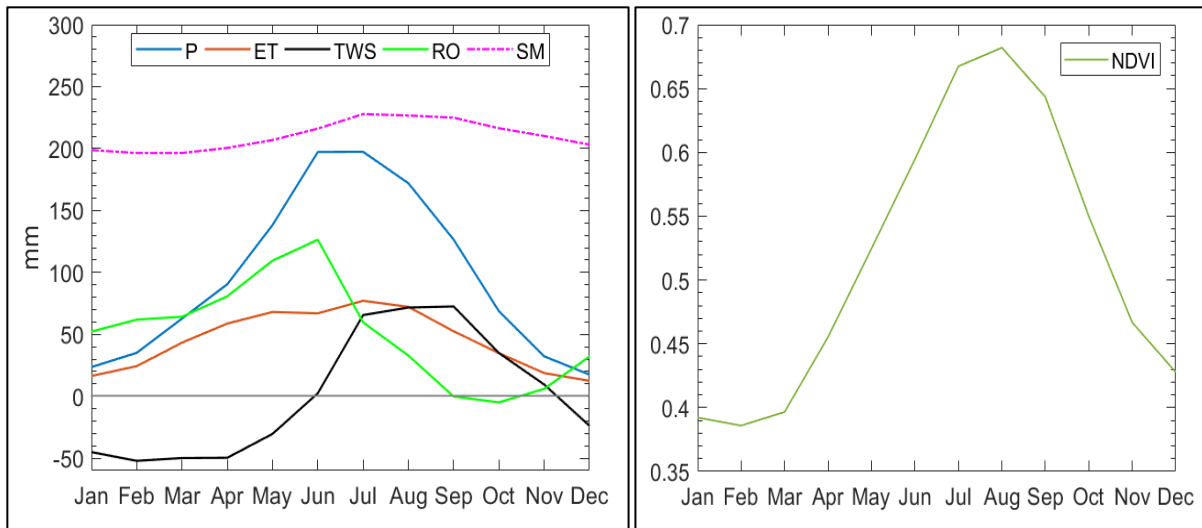


Figure 5-1: Basin mean-annual monthly changes in P, ET, TWS, RO, NDVI and SM over the Yangtze Basin. RO is the calculated runoff from the water balance closure.

In Figure 5-1, P, and ET patterns follow annual seasonal trend peaking between June-August before receding to the lowest in winter, December-February. June-September is the summer (rainy season). Mean basin precipitation is 1106.4mm and corresponds to the literature range of 1060-1180mm and in-situ measurements (Wang et al., 2011). Mean annual ETa is 545mm, close to literature value of 530-560mm (e.g., Wang et al., 2011) and follows a similar pattern as P and NDVI, peaking in July before gradually declining to a minimum in Dec-January. June-August has the highest values of NDVI, P and ET corresponding to the summer growing season. The NDVI peaks in August, a pointer that the vegetation lags P by a month. TWS is low, ± 50 mm, from January to March (winter) and is maximum in summer July-September before gradually retreating to antecedent levels by December. The TWS pattern coincides with Qian et al. (2010) findings for the same basin. RO increases as TWS decreases and is maximum in June; when P is maximum.

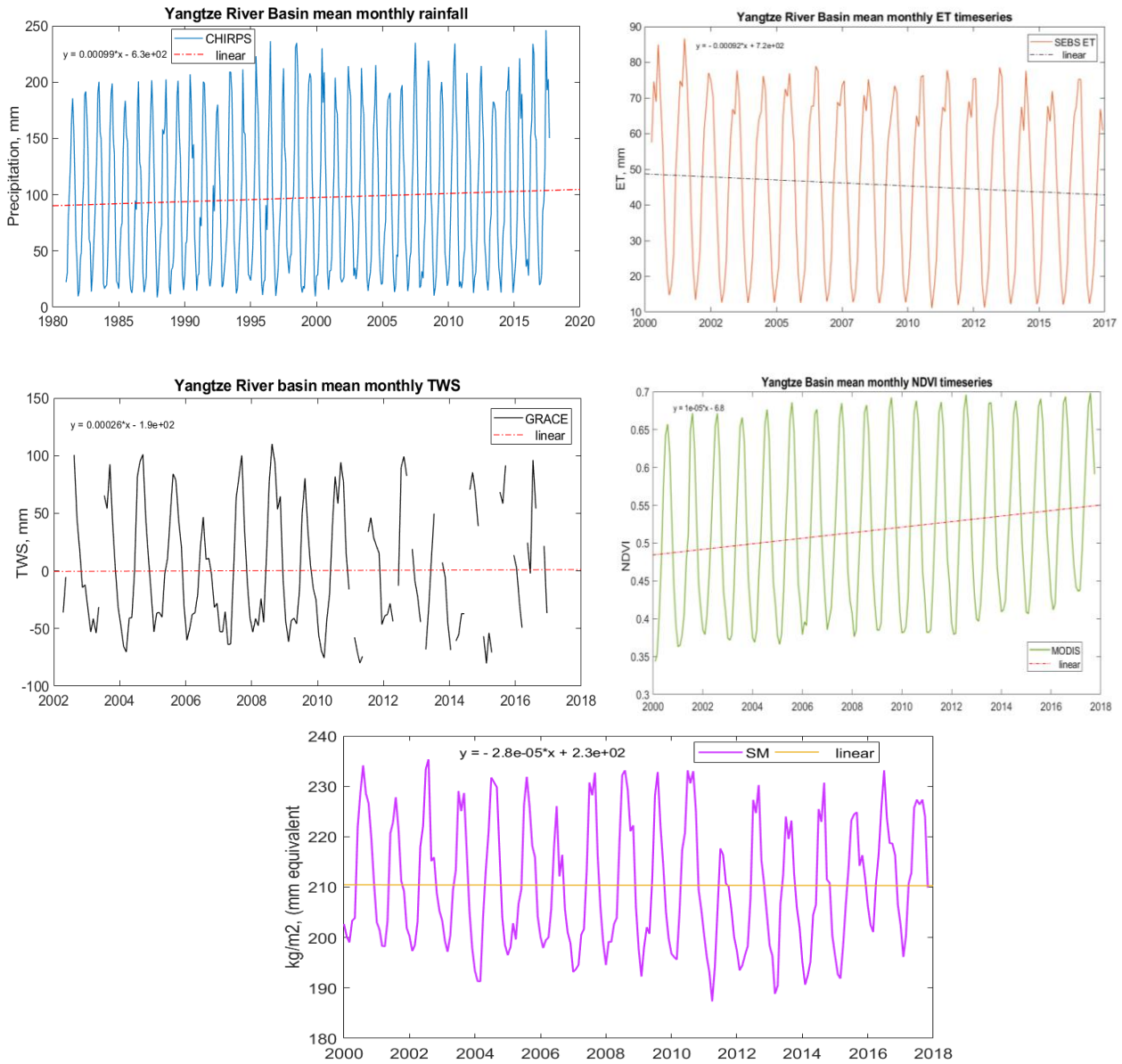


Figure 5-2: Basin mean monthly precipitation, ET, TWS, NDVI and GLDAS SM time series

In Figure 5-2, all but the ETa basin monthly means show increasing trend over the years gaining 10-22%. Empirical mean precipitation in the basin increased by approximately 20mm since 1981, NDVI by 0.07 since 2002 while TWS increased by about 10mm since 2002. NDVI increase agrees with Zhang et al. (2010) findings for the same basin explained as due to government policy on water and soil protection measures (reforestation) and increased built-up environment (green cities). TWS increase agrees with (Huang et al., 2015) findings, explained as due to anthropogenic modification of the TWS as a result of intensive surface irrigation. ETa, however, shows a decreasing trend at about -5mm since 2002. The ETa decrease corresponds to Wang, et al. (2011) findings indicating decreasing trends in decadal annual mean actual evaporation by -3.6 mm (10yr)⁻¹ in the whole of the Yangtze River basin, -1.6 mm(10yr)⁻¹ in the upper Yangtze reaches, and -5.8 mm (10yr)⁻¹ in the mid-lower reaches. The deduction is that over the years, changes in the saturation vapor pressure deficit (SVPD) have altered, and the wind speeds decreased (Liu, Xu, Henderson, Qi, & Li, 2004; Y. Wang et al., 2011). Additionally, cloud cover/aerosols have increased with a consequent that, effective net solar radiation in the basin has reduced. A combination of reduced

wind speeds and reduced net radiation has a consequent that ET_a reduces. Increased P is a function of shifts in regional air mass movement and the monsoonal influences. Large water reservoirs like the Three Gorges Dam may alter weather patterns and trigger formation of micro-climates with a consequent that precipitation received in area increases. Thus, the increase in precipitation received in the YRB over the years.

As seen Figure 5-2 the mean monthly TWS is low from late 2005-mid 2007 changing at between ± 50 mm; against the normal range of +100mm in summer and -50mm in winter in other years. A similar anomaly is seen in late 2009-2012. Over the same time, for the period between late 2005-mid 2007, the summer SM is -5mm lower than in other years and is even lower in late 2009-2012. Furthermore, the two figures are similar in pattern and trend. The anomalies coincide with three key events in the YRB: the 2006/07 drought, year 2004-2008, the period when TGD was being constructed and filled, (Huang et al., 2015; Su, Timmermans, et al., 2017) and the period after the reported 2009-2010 drought (Hook, 2011; Huang Wei, 2017; OMT, 2012).

These anomalies are explained as that the filling of the Three Gorges Dam reservoir increased storage upstream of the dam (the upper reaches) and reduced storage downstream before gradually returning to the average levels afterward (Su, Timmermans, et al., 2017); an indication that construction of dams across water systems influence water balance components. Although drought is reported in 2009/10 (Hook, 2011; Huang Wei, 2017; OMT, 2012) subsequent deficits in TWS and SM are not drastic/immediate for the same period but manifest later, between 2010-2012. Human activities such as increased irrigation modify the water cycle and is reported (Huang et al., 2015) since 2003. It is therefore likely that following the 2010/11 drought, farmers resorted to largescale irrigation. With increased abstraction and reduced rainfall, net outflows from the basin exceed the inflows resulting in deficits, seen as lags in SM and TWS mid-2010-2013. The significance of this is that effects of meteorological drought are immediate, affect the food supply and cause short-term human-discomfort. However, hydrological drought and impact on water resources is slow and may take longer to manifest.

Considering the basin mean annual changes TWS and the NDVI with respect to P, Figure 5-1, NDVI peaks in August and corresponds to the month when the TWS is the lowest; an indication that NDVI and TWS lag precipitation by a month. Consequently, SVI and STWSI were lagged by a month against the SPI and SPAEI to account for the time delay for vegetation and the terrestrial water storage responds to precipitation events.

5.2. Quality control

5.2.1. SVI standardization

Figure 5-3 shows the variation of SVI time series with respect to the SPI and SPAEI at a pixel within the basin. The SVI is mostly discordant to the SPI and SPAEI at different timescales an indication that SVI does not directly respond to changes in precipitation and ET.

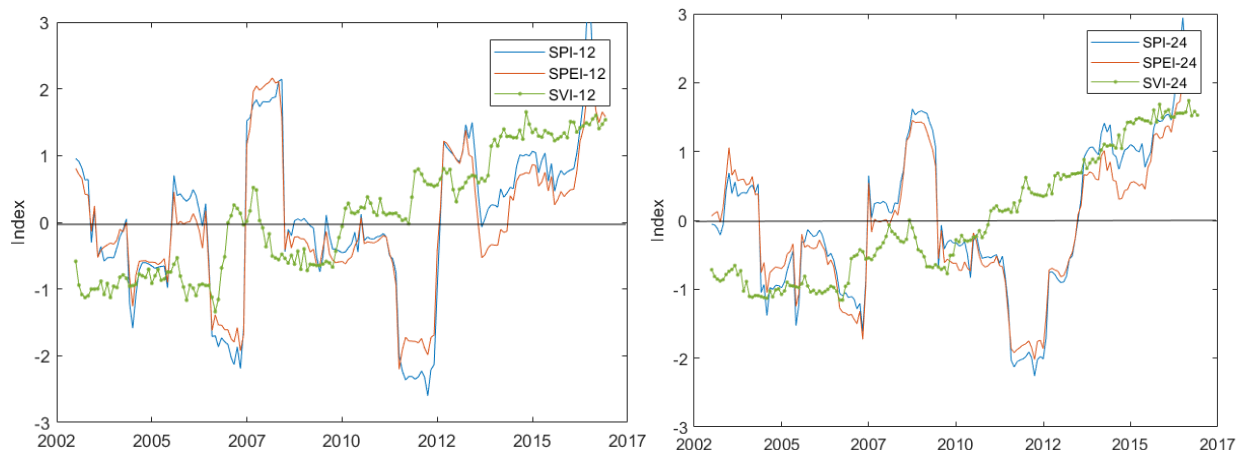


Figure 5-3: SVI variation w.r.t SPI, SPAEI and the STWSI at a pixel within the basin.

Figure 5-3 suggests that the NDVI has increased consistently over the years. A similar observation as in the earlier time series of NDVI, Figure 5-2 mostly in the summer month, while there was no change in the winter months. This suggests that NDVI is not limited by the drought, but responds to some other development such as increased agriculture or natural greening due to some other factors such as land use change, urbanization, increased cloud cover due to smog/aerosols, light, carbon dioxide and temperature etc. At the same time, ET decreased due to meteorological forcing as explained in section 5.1.

The discordance in the SVI time series was explored further by normalizing the NDVI data using the GEV following the same standardization procedure used for the SPAEI as a check to confirm goodness of the SVI standardization. SVI results obtained with GEV standardization method approximates and agree with those obtained through normal standardization well. SVI/SVI-gev correlation is greater than 0.98 in all instances and proved the sufficiency of the normal standardization procedure. Of note is that, although GEV seems to exaggerate spurious instances especially the tails the differences are small (Figure 5-4).

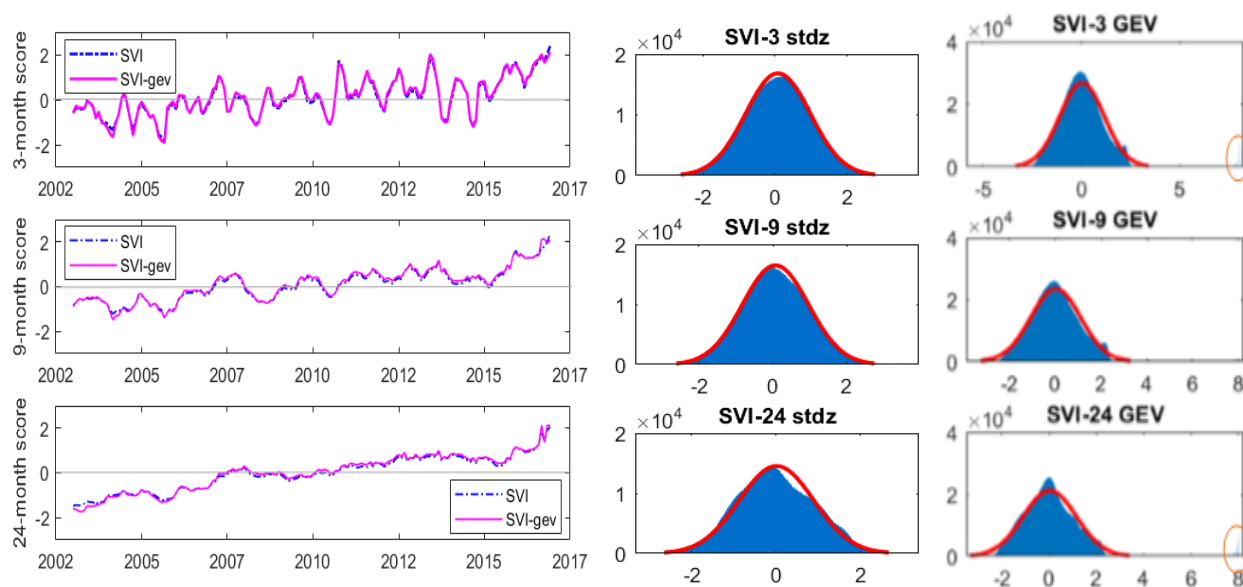


Figure 5-4: Time series and histogram fits comparing SVI results obtained using normal standardization to those obtained using standardized the GEV

5.2.2. SPAEI and SPI standardization

As a check and to confirm the efficacy of the SPAEI, the calculated SPAEI-1 and SPI-1 were compared to existing SPEI-1 obtained from the Global SPEI database (*SPEIbase v2.5:1 dataset*)³ maintained by Vicente-Serrano et al. (2011) and is presented in Figure 5-5. The years 2003, 2006, and 2010 are widely reported as drought years. Subsequent analysis is based on the years 2003, 2006 and/or 2010.

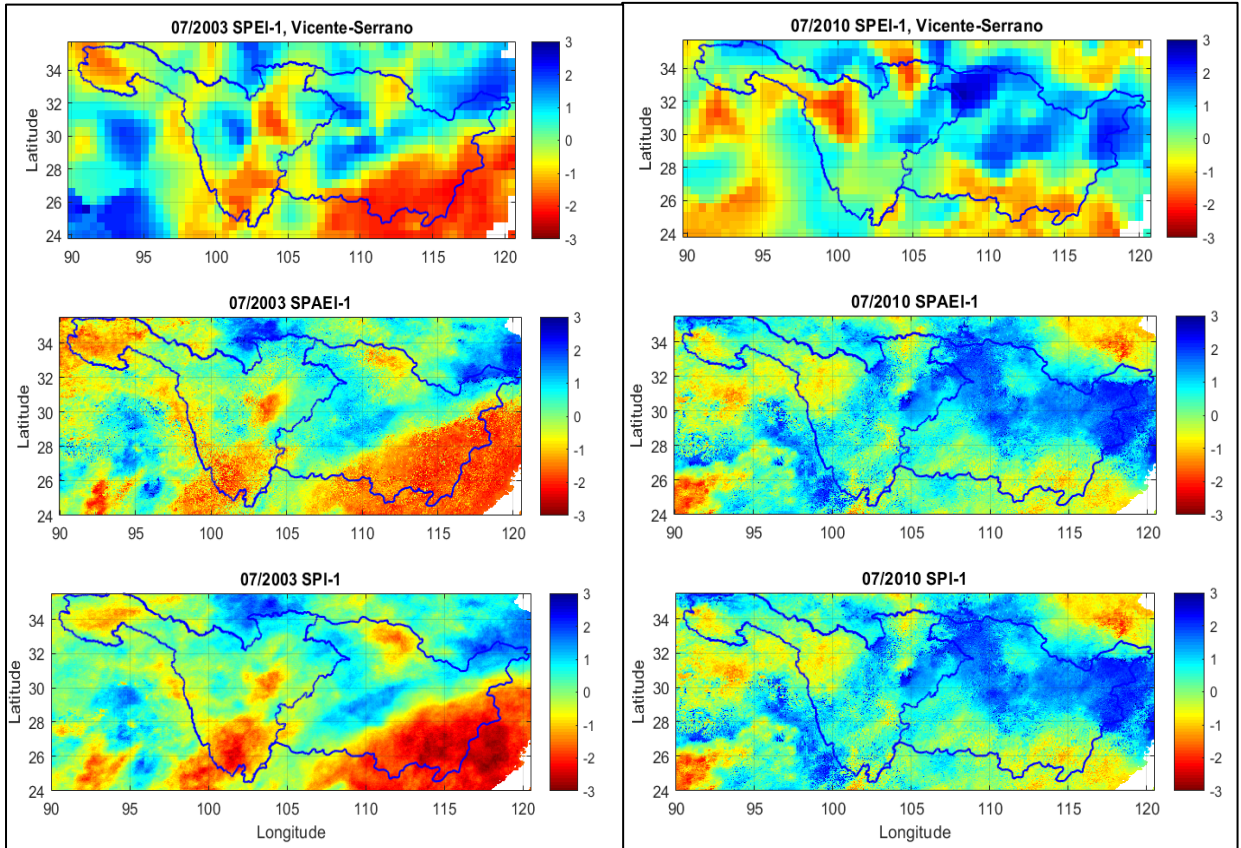


Figure 5-5: Spatial comparison of the calculated SPI-1 and SPAEI-1 to existing SPEI-1 (SPEI database 2015) July 2003 image

The SPEI-image is at a coarser spatial resolution (0.5°) than the finer (0.05°) SPAEI and (0.05°) SPI. Despite the spatial resolution difference, there is striking semblance in the spatial drought pattern, distribution, variability and magnitude (*wet: 0 to +2.5, drought: between 0 and -2.3*) as captured by the three. This confirms the calculated SPAEI and SPI results were comparable and reliable. Differences arising, therefore, are a consequent of scale issues and spatial heterogeneity.

³ <http://spei.csic.es/database.html>

5.3. Comparison of the SPI, SPAEI, SVI and STWSI

5.3.1. Statistical analysis

Pearson correlation coefficient (r) correlation analysis was done establish how the indices were related to each other at different time scales. This was done by convolving the spatial averages of the SPI, SPAEI, STWSI and SVI time series data against each other for the period January 2003-Dec 2016. The goodness of distribution was assessed through scatter diagrams and qq-plots.

The indices are positively correlated to each other except for SVI against STWSI series. Correlation is highest in the SPI-SPAEI time series at all time scales ranging between 0.83 and 0.97. SPI-SVI correlation ranges from 0.3-0.7. Correlation of the STWSI to other indices is low ranging between 0.03-0.75 when positively correlated and between -0.39 to -0.01 against the SVI. Figure 5-6 is a representative sample obtained for Cuntan area and shows the correlation of the 6-month SPI against and the 6-month SPAEI and SVI. The SPI-6/SPAEI-6 correlation is 0.901 compared to 0.471 with SVI-6. Scatter is minimal with SPAEI and larger among the SVI and STWSI.

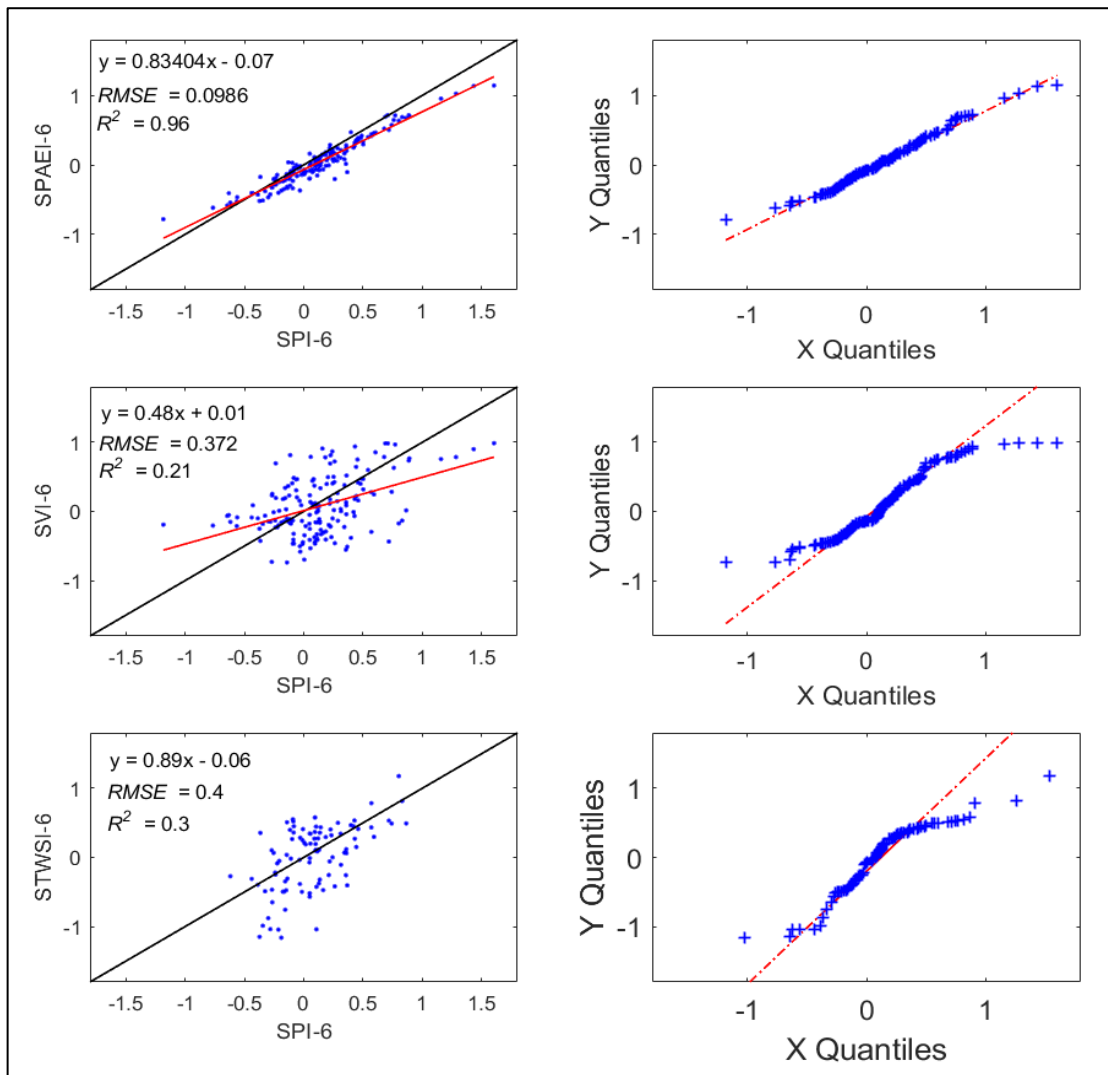


Figure 5-6: A scatter plot showing the correlation between SPI-6 and SPAEI-6, and SVI-6 and QQ-plots showing the distributions. Degrees of freedom in the SPI-STWSI=96; against 166 with SVI and SPAEI

To optimize the relevant drought monitoring length, a correlation matrix Appendix 1 and Appendix 2 was prepared. For this, the Pearson correlation coefficients between paired spatial-averaged time series of the severity values estimated using the indices at different timescales were computed based on Jain et al. (2015). For example, SPI-3 was convolved against SPAEI-3 severity values, and correlation coefficient (0.89) was computed for the pair to form a cell of the matrix. Similarly, SPI-1 was paired against other DI's for all time steps and so on, resulting in a cross-correlation matrix with 24 rows and 24 columns. The coefficients were then averaged and compared to derive the optimum monitoring length.

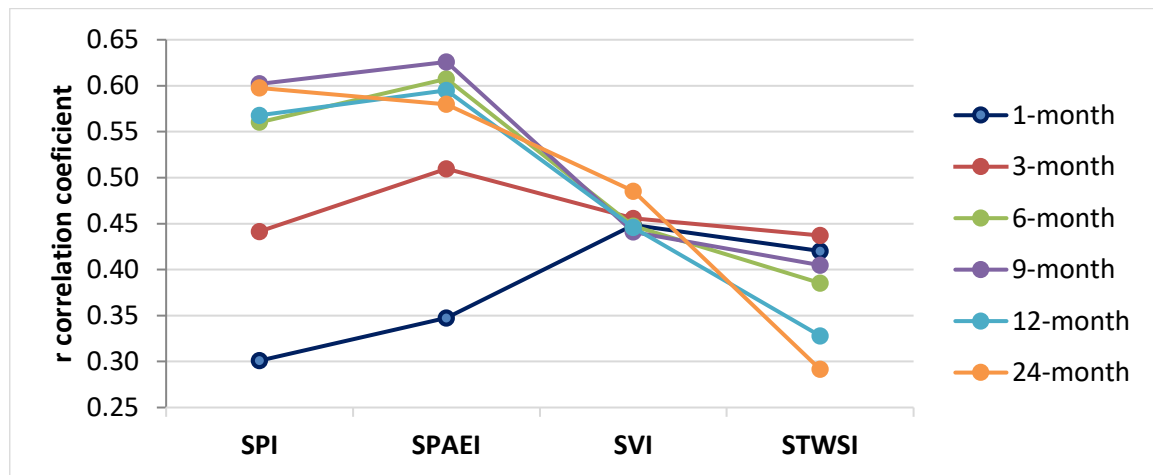


Figure 5-7: Average correlation derived from the correlation matrices by averaging the coefficients at different scales.

Figure 5-7 shows the results of the average correlation coefficients derived from the correlation matrix. It is observed that correlation increases with longer time-steps such as (6-12 months) and is low at 1-month in all indices, a finding that agrees with (Jain et al., 2015). All but the SVI show variability and wide range response. SVI show subtle variation ranging from 0.4-0.49 and fall below the $r > 0.5$ significance threshold. SVI is a function of the NDVI and like other NDVI based indices, it's affected by other factors like crop phenology, crop type, irrigation, etc. and is not directly related to precipitation. Also, probably because the NDVI is already a normalized signal, fluctuations are subtle.

SPI and SPAEI are best correlated at 9-month time-step. Correlation is lowest in STWSI time series and fall short of the $r > 0.5$ significance threshold. However, there is higher variability and wider response with the STWSI, and is best correlated at 3-months with others. Low correlation in STWSI is probably due to the difference in trend between TWS and shallow water storage. Also probably due to missing data and gaps in the GRACE TWS data.

Drought indices computed at 6-12month time step are best correlated with each other an indication that 6-12month is the optimal drought monitoring length. Correlation is highest at similar time steps and least at dissimilar time steps. This finding agrees with Jain et al. (2015) finding that 6-9month is the optimum monitoring length.

5.3.2. Time series

To assess the performance of the drought indices, respective time series were compared to identify drought onset and duration; defined when the scores are consistently negative. This was done in two parts. Using the time series representing the Cuntan area (pixel 116,330) shown in Figure 5-8 and Figure 5-9 and using the

spatial basin averages, Figure 5-11. The results are presented under subsections: (a) SVI-SVI-gev, (b) SPI vs SPAEI, combined time series for Cuntan area vis-a-vis the combined time-series for the basin.

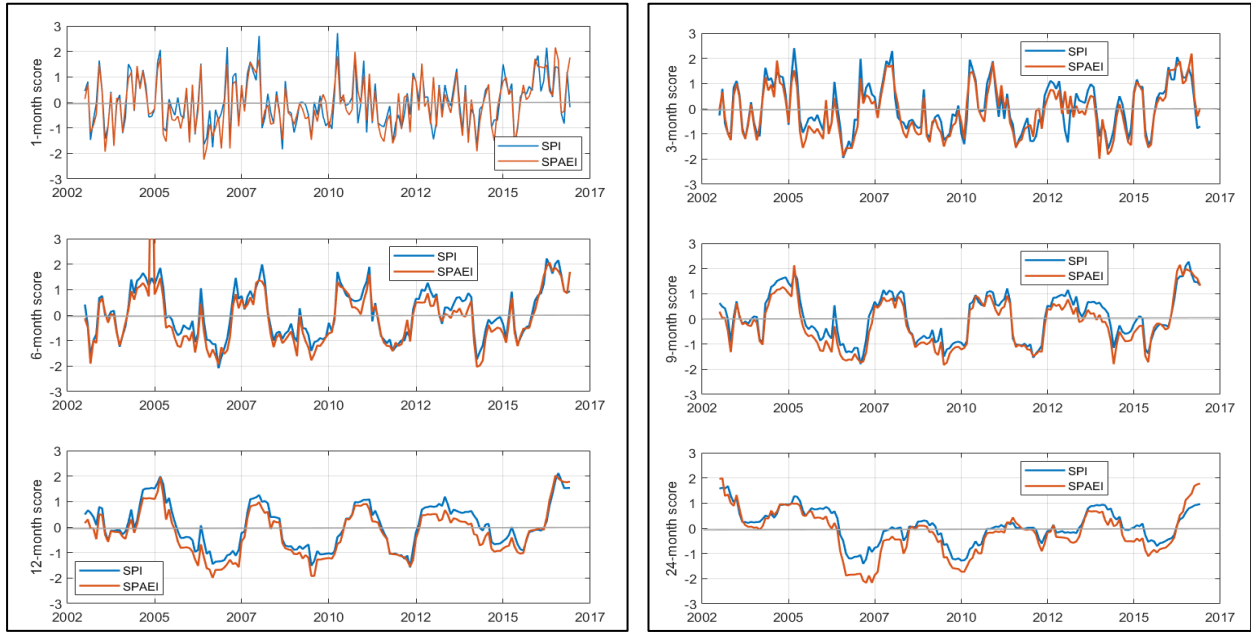


Figure 5-8: Timeseries of the SPI vs SPAEI from 2003-2016 at pixel (116,330).

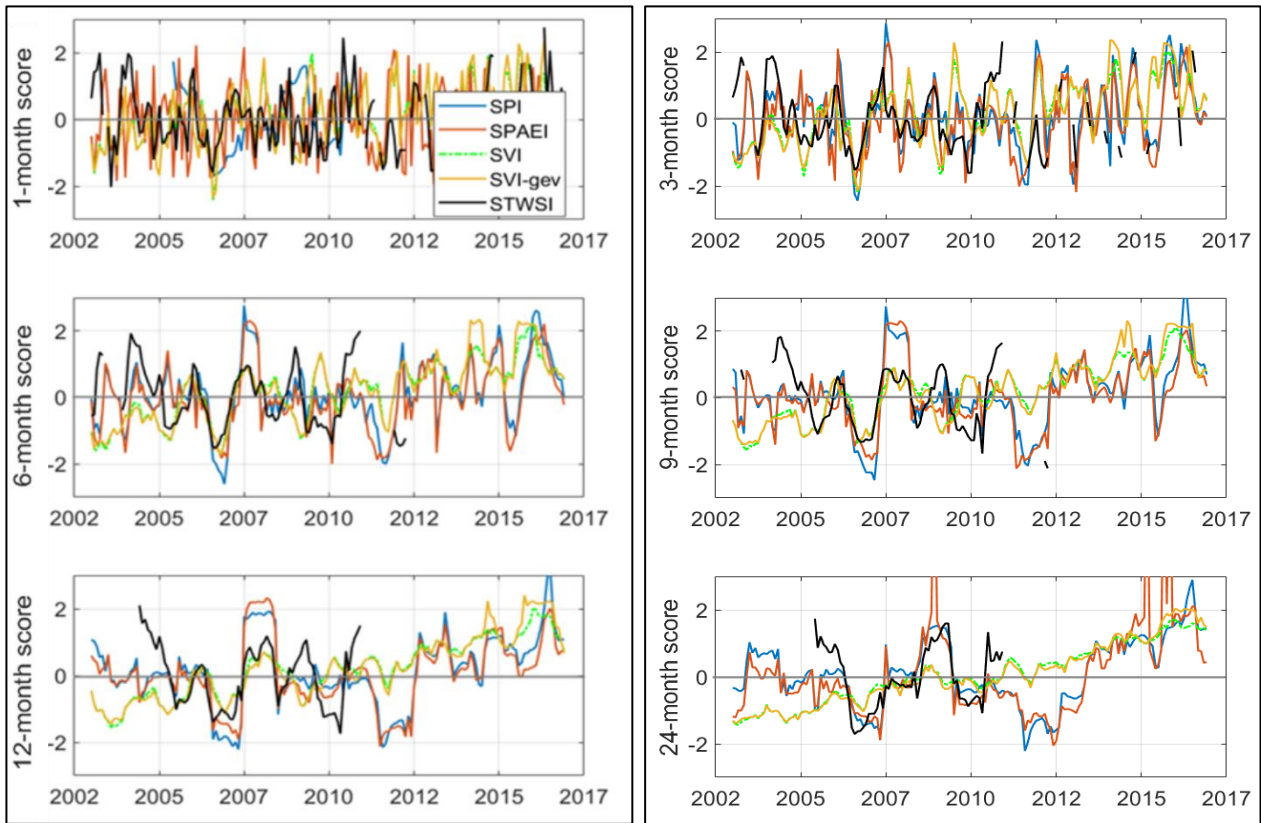


Figure 5-9: SPI, SPAEI, SVI and the STWSI timeseries for Cuntan Gauging Station from 2003-2016

a. Variation of the SVI with SVI-gev:

From Figure 5-4 there is good agreement between SVI/SVI-gev that is maintained throughout the timescales. Results of the cross-correlation between the corresponding time series of SVI/ SVI-gev and SPI/SPA EI, correlation coefficients above 0.98 were obtained and are significant at the 95% confidence level.

b. Variation of the SPI against SPA EI:

Figure 5-8 shows the time series of the SPI and SPA EI over the study period at a randomly picked pixel in the basin. The two indices follow the same pattern, are quite similar and capture drought events adequately. They are also highly correlated to each other throughout the timescales especially at similar time steps posting correlation coefficients as high as 0.97, in the 6-12-month time step as seen in Figure 5-10. Nevertheless, there are considerable differences in how they capture the magnitude, severity, and onset of some events. The SPI appears to overestimate the wet periods and underestimate some of the severe drought events. Two instances where this happens is between in 2006 summer drought and in the 2009/10 winter drought. The difference arising from the fact that the SPI does not factor for evapotranspiration variability and depends solely on precipitation. Therefore, extreme events in the rainfall time series will result in subsequent overestimation of wet periods or underestimation of drought periods by the SPI. Additionally, when ET is higher than the precipitation, drought conditions intensify and the SPA EI signal would appear larger.

Like the SPEI, SPA EI is a better drought predictor than the SPI as it incorporates ET variability (Beguería et al., 2014; Homdee et al., 2016). SPA EI, therefore, captures intense (higher magnitude) and severe drought events better. However, the differences are subtle. Only in the early 2000's where it is clear that the SPI captures drought onset earlier than the SPA EI. A possible explanation for the delay/lag in the onset is low evapotranspiration over the period.

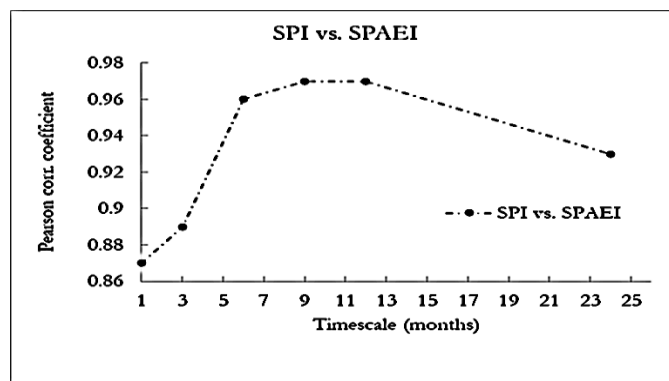


Figure 5-10: Correlation between SPI and SPA EI series

c. Variation of the STWSI against SPI, SPI and SVI

Figure 5-9 shows the combined time series of the SPI, SPA EI, SVI/SVI-gev and STWSI at select timescales for Cuntan area. SPI, STWSI and the SPA EI generally depict good agreement with each other at larger time scales (greater than 6 months). The three indices capture comparable drought events on shorter-time-scales, despite subtle differences occasioned by the TWS lag. For instance, the STWSI captures the 2006/07 summer drought and longer drought event of 2009/2010. However, discordant instances are noticed against the SPA EI at 1-month scale. While the STWSI, SPI and SPA EI capture the short-term 2010 drought and

the severe 2010/11 winter drought experienced in China SVI-12, 24 entirely misses the event and appears incoherent and disjointed. Generally, SVI series follow a three-cycle evolution character. It is consistently negative between 2003 and 2007, oscillates close to zero from 2007 to 2012 and is above zero from 2012 onwards. Despite the discordancy, the crests and troughs of the SVI series are comparable and captures drought events adequately for timescales less than 9-months. For instance, like the rest, SVI-1, 3 and 6 capture the short term 2003, 2006 drought and the long-term 2010/11 events. The SVI-9, 12 and 24 missed the 2010/11 event.

d. Comparison of the basin means of the SPI, SPAEI, STWSI and the SVI:

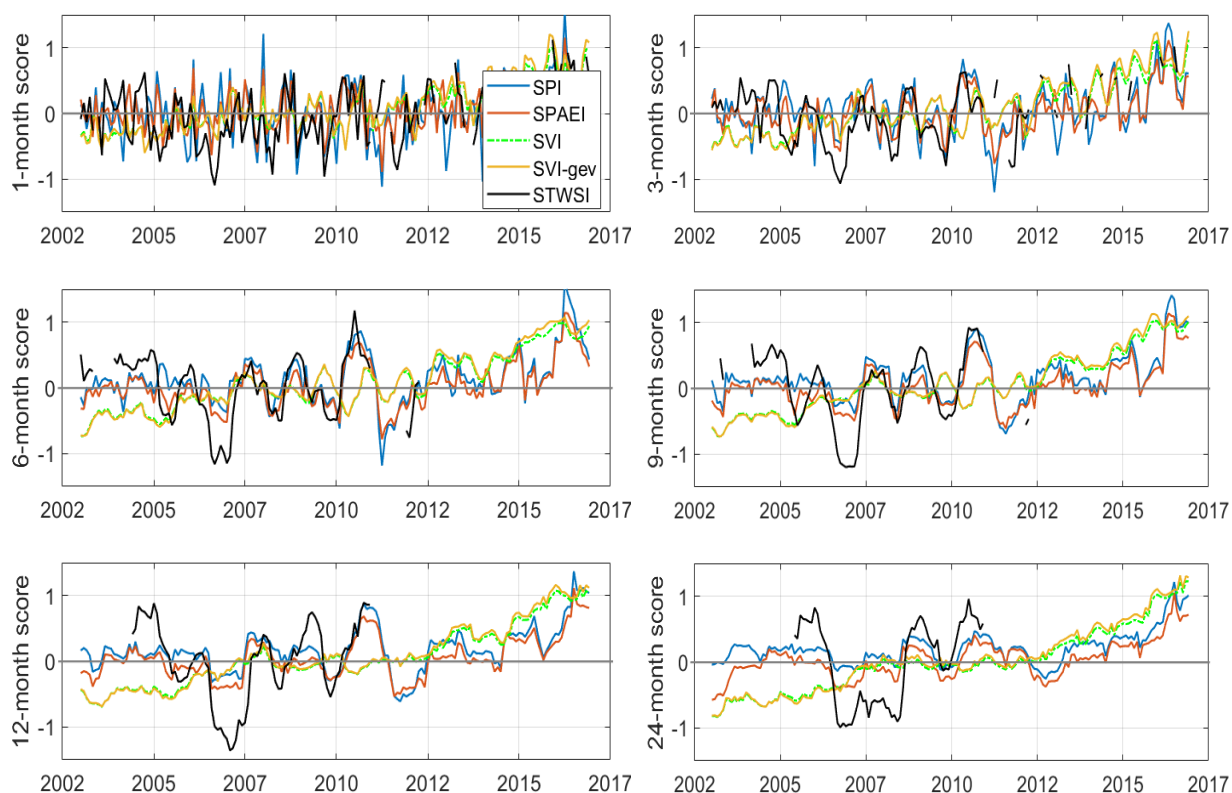


Figure 5-11: Timeseries of the SPI, SPAEI, SVI and the STWSI over a fifteen-year period (2003-2016) for the Yangtze River Basin.

From Figure 5-11 the basin mean SVI time series exhibit three-phase evolution character and responds slowly to changes in P and ET. From 2003-2007, the basin mean SVI is continuously low (below zero) suggesting prolonged normal-drought of magnitude <-1 and appears entirely decoupled from changes in P and ET. The second phase runs from 2007-2012 during which the SVI oscillates close to zero. Here, the SVI appears to respond well to changes in P and ET (SPI and SPAEI) for time steps below 12months. However, between 2010 and 2011, SPI-12, SPEI-12 and STWSI-12 are more than zero when SVI-12 is <0 . The third phase is between 2012 and 2016; when all are above zero. However, the SVI is consistently higher than the two. Mainly, the SVI series are mostly discordant to the behavior and pattern of the other indices a likely indication that vegetation sensitivity is not linear and that SVI responds slowly to precipitation. However, despite non-synchronous pattern, the crests and troughs of both SVI and SVI-gev time series

follow the TWS, SPI and the SPAEI at shorter time steps (less than 9months), an indication that SVI is most suitable for short-term drought monitoring.

The STWSI show larger amplitudes and drought intensity than the SPI and SPAEI, a probable indication that the deficits are a function of deep-groundwater recharge. The results indicate that drought indices based on different variables show the same major drought events. Drought indices based on precipitation and potential evaporation are more variable in time while drought indices based on NDVI and groundwater have a smoothed signal.

In Figure 5-11, basin averages of the SPAEI, SVI and the SPI show above zero values from 2012-onwards with the SVI. The NDVI and precipitation received in the Yangtze basin have been increasing since 1981(Chen et al., 2014; Zhang et al., 2010). So the increasing trend is synonymous with literature.

5.4. Drought Assessment: Spatio-temporal drought evolution

Map series were used to present spatial-temporal drought variability at different timescales as captured by the indices for the period 2003 to 2016. Winter (January) and summer (July) map-time series for the year 2006 and 2010 are compared and presented in Figure 5-12 through Figure 5-15 showing drought evolution as captured by the four indices at 3, 9 and 24-months. The 1, 6, and 12-month maps are included in Appendix 5 and Appendix 6. Red indicates water-stress, and blue represent wet conditions.

The indices drought sensing capability differ as seen in the maps. Summer drought was experienced in 2006 and in 2010 winter drought. Thus, July 2006 map series appear drier, intense and widespread than in 2010 for the same month. A similar pattern is seen in Jan 2006 an indication that both the winter and summer droughts were experienced in 2006, unlike in 2010 where wetness is seen in July and dry in January. Mostly, drought was widespread across the mainland and areas to North. Rainfall in 2006 appear concentrated in areas closer to the sea (Southeast corner) suggesting convective rainfall.

The indices show good spatial correspondence despite discordant instances with the SVI and STWSI. STWSI pattern is distinct around 25-30°N, and 100-105°E SPI and correspond to SPAEI and SPI pattern for the same region SPAEI and SPI patterns are consistent with each other at all time-steps and also agree with STWSI series longer timescales. The differences are largely occasioned by spatial scale mismatch and spatial heterogeneities in GRACE data against other datasets. SVI, on the other hand, doesn't show drastic changes and variability with meteorological factors and agrees with Zhang et al. (2010) findings for the same basin. NDVI in the Yangtze Basin has been increasing over the years, and Zhang et al. (2010) gives a possible explanation for this as (a) government policy on water and soil protection measures (reforestation) and (b) presence of built-up economy (green cities). From the maps it is evident that the indices capture drought differently over times. Against the SVI, areas in the midstream show no obvious fluctuations with the meteorological factors change. Nevertheless, SPI and SPAEI results are very similar, because they are derived on similar inputs.

Additionally, since rainfall falls in summer, deficits in summer would have a long-term effect on water-resources before the next rainfall cycle (at least 12months apart) and would be devastating. Winter drought is short-term, and its effects would be subdued by the summer rainfall in June. The results are consistent with the SDI time series, in Figure 5-8 and Figure 5-11.

January 2006

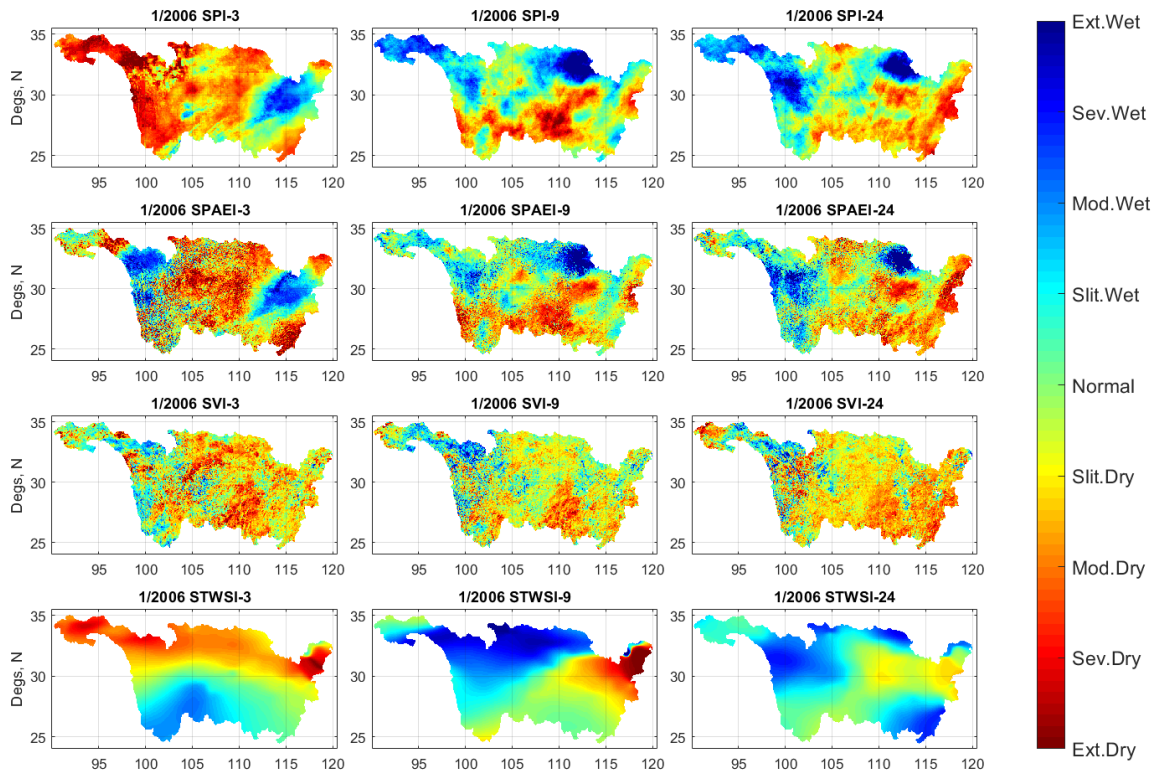


Figure 5-12: Comparison of drought as captured by the 3, 9 and 24-month indices in Jan 2006

January 2010

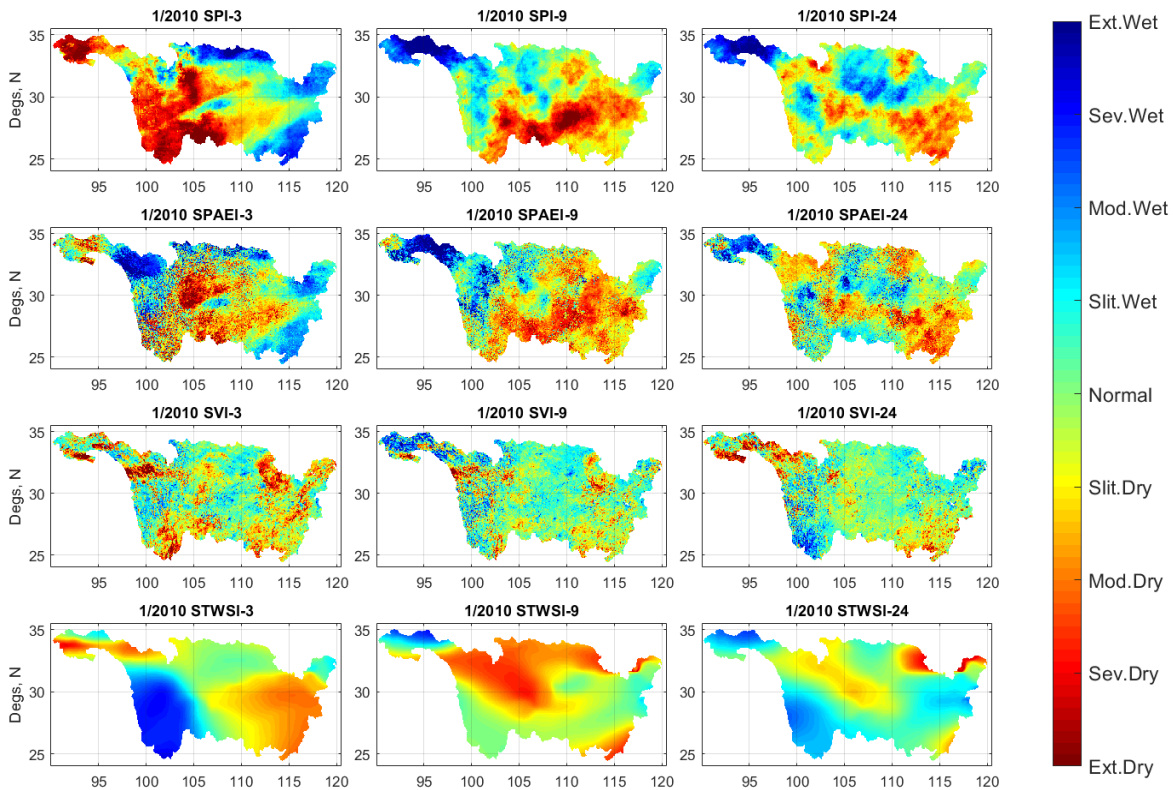


Figure 5-13: Comparison of drought as captured by the 3, 9 and 24-month indices in January 2010

JULY 2006

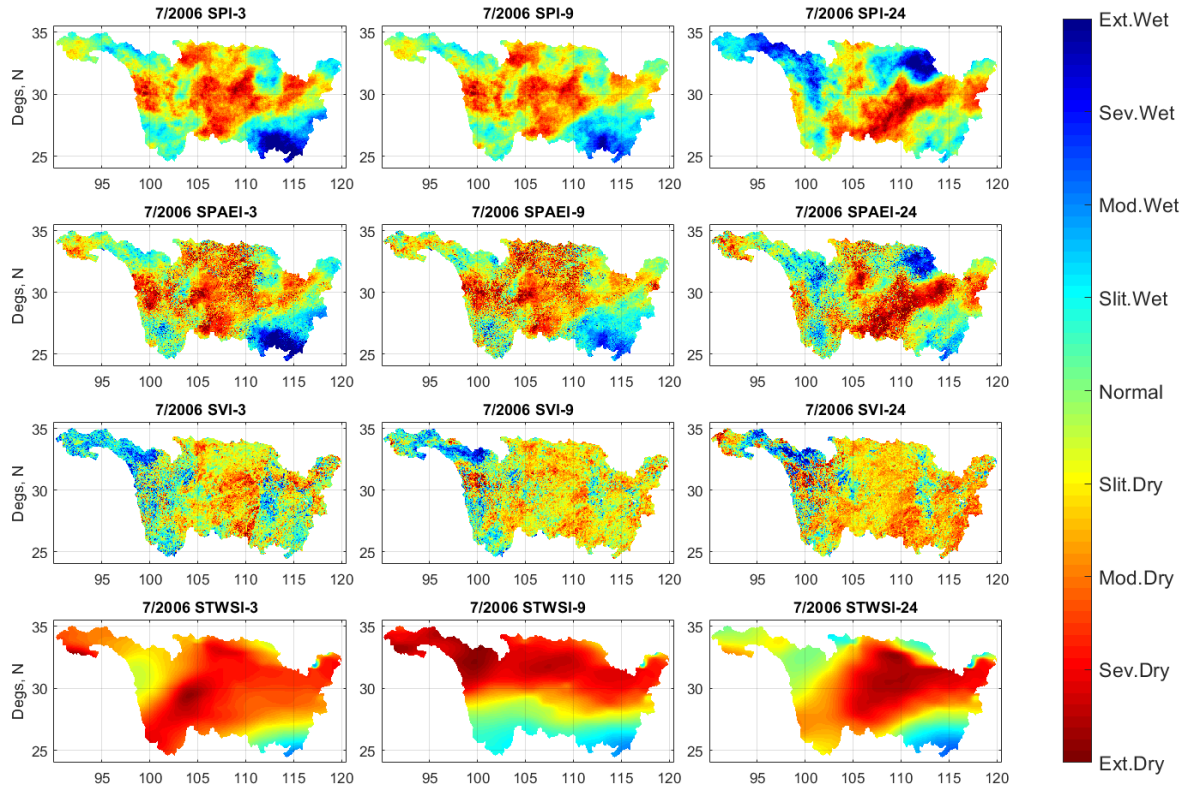


Figure 5-14: Comparison of drought as captured by the 3, 9 and 24-month indices in July 2006

JULY 2010

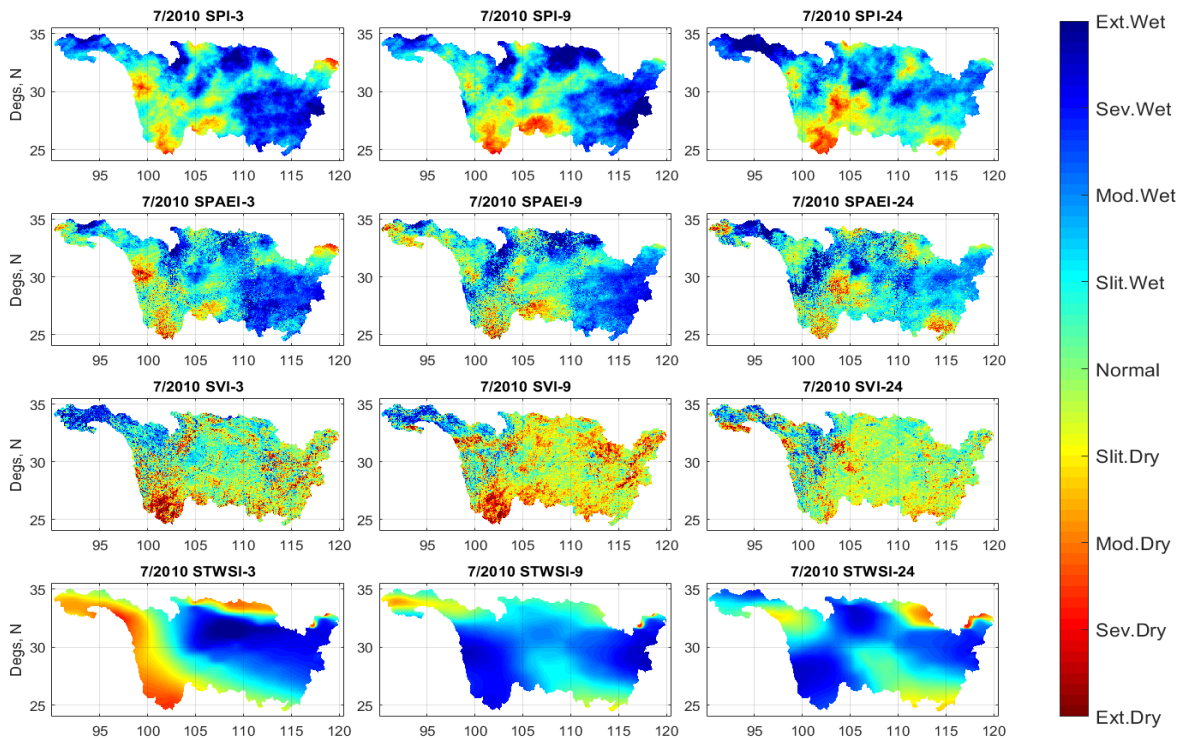


Figure 5-15: Comparison of drought as captured by the 3, 9 and 24-month indices in July 2010

Discussion

The time-series drought maps generated with the indices indicate that meteorological, hydrological and vegetative droughts are not linearly correlated with one another and respond to other forcing other than meteorological. From, Figure 5-2 the NDVI show increasing trend over the Yangtze as ET_a reduces. ET_a reduction as explained earlier as probably due a reduction in wind speeds and reduced net radiation due to clouds/smog or increased urban developments. Increased NDVI is associated with government policy and restrictions on trees, increased agriculture, and change of land use and development of green cities. Thus, SVI show slow response to meteorological forcing and is in line with Anyamba & Tucker (2012), that vegetation canopies saturate the NDVI relationship and are not bound to precipitation changes. This explains the slow variation of SVI to the other indices.

STWSI and SPI and SPAEI infer the most dominant component of the hydrologic cycle. Correlation is maximum at shorter scales i.e. the 3month and 1-month timescale when the hydrological cycle is dominated by changes occurring at shallow depth and is maximum at >6 month SPI/SPAEI when the hydrological cycle changes at depth. The STWSI is sensitive to changes occurring in the TWS and changes occurring in extending beyond the root-zone SM to the deeper horizons of the groundwater. On the other hand, SPI and SPAEI track changes happening on the earths' surface as influenced by temperature and ET. At short-scale, the STWSI infer surface water changes (shallow depth). Thus, the three indices show similar response at 3- month step. However, at longer scales, the relationship is inverse, as seen in (Figure 5-15), STWSI show no drought (blue) whereas SPAEI and SPAEI show drought (red). This is because, at longer-scale, after the precipitation has ceased, water is only available as groundwater. The speed of drought development and drought duration are also different in different spheres. Therefore, it is quite common that where a drought index identifies a drought, another index misses it as seen in the maps.

5.5. Water Balance

The water balance approach was used to estimate the runoff from the Jialin-Mintuo-Jianshi sub-catchment within the upper reaches of the YRB, as the residual of the water balance equation, using estimation steps explained in section 4.5. The calculated runoff was then collated against observed discharge measurement obtained from Cuntan gauging station for the period 2005-2010 and are presented in Figure 5-16.

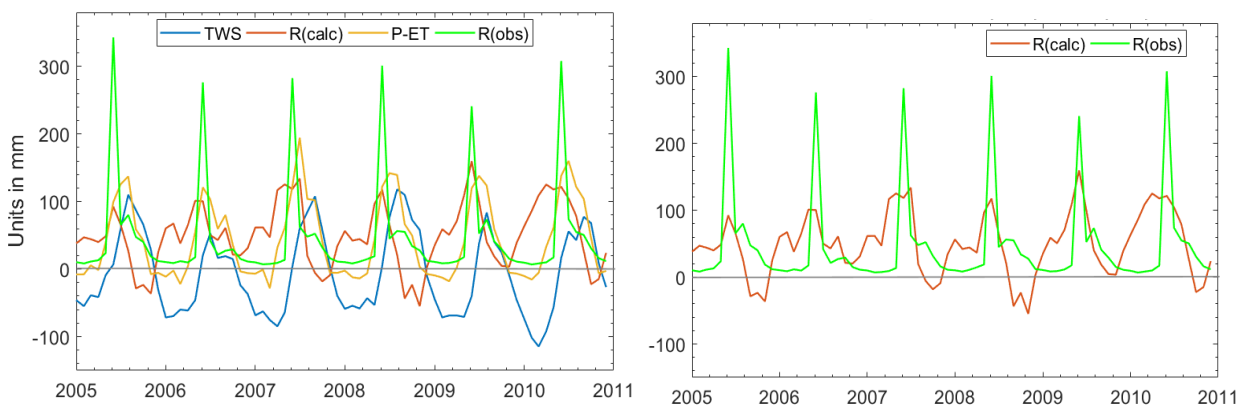


Figure 5-16: Relationship between TWS, calculated runoff (Rcalc) and discharge measurements (Robs) at Cuntan Gauging station from 2005-2010.

As seen in Figure 5-16 the water balance components are consistent with each other and maintain a seasonal pattern; an indication that the dynamics of the surface water cycle fluxes are adequately captured. The peaks of the R(calc) and the R(obs) coincide in June, and there is a considerable agreement in the rising and falling limbs of the two series. However, the peaks of R(obs) are spikier than in the R(calc). R(obs) measurements were obtained from the Cuntan Gauging station at the entrance to the Three Gorges Dam and located about

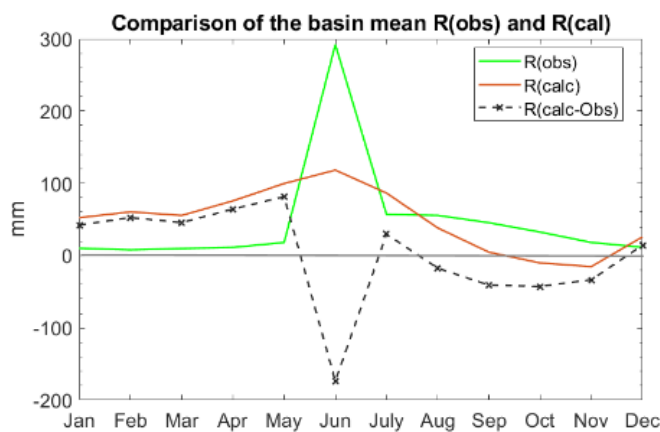
600km from the outflow gates of the dam. For flood control, water is released from the dam in June(S. L. Yang et al., 2010) to lower the water level in the upstream reservoir to accommodate the runoff generated in the hinterland upstream of the dam over the period (summer-spring) and explains the sudden spike in the June R(obs) series.

Changes in TWS are fluctuations in water storage: surface, soil, snow, groundwater and infer deep groundwater dynamics (Huang et al., 2015; Qian et al., 2010). Intrinsic to water movement through a catchment, TWS behavior depends on catchment characteristics: slope, soils, geology, land cover and the seasonal snow dynamics. Unlike P and ET, TWS changes are slower and lags P and ET and in this case by a month, as seen in Figure 5-16. Positive TWS anomalies represent periods of net system recharge (runoff) while negative TWS values represent leakage/loss due to evapotranspiration and anthropogenic withdrawals (Forootan et al., 2017; Huang et al., 2015; Strassberg, Scanlon, & Chambers, 2009). Runoff is generated whenever P exceeds ET and the soil storage capacity, as precipitation percolates.

In winter, P and ET are minimum, and TWS recedes to below zero. TWS decreases as water leaves the catchment (water release as groundwater or as surface runoff) resulting in a subsequent increase in the R(calc). This happens in winter through spring. TWS gradually increases through the monsoon and is maximum in August as P replenishes the released winter flux. Discharge is concentrated in one period, possibly when the reservoir is being filled.

Comparing the R(obs) to R(calc) in

Figure 5-17, calculated runoff generally overestimates runoff in winter through summer except for June where the observed runoff is twice the calculated runoff due to the dam-water release. R(calc) underestimates Robs in autumn as water accumulates. The water balance does not close. However, despite lack of closure, the difference between the accumulated annual R(calc) and R(obs) is minimal (620mm against 570mm) and the mean bias error in the annual runoff was 8.85% although was larger on month-month. The discharge is significantly low October-November as water is stored for later release and agrees with (Chen et al., 2016) findings for the same basin.



Month	R(calc)	R(obs)	RBIAS (%)
Jan	52.2	10.2	411.8
Feb	61.9	8.0	673.8
Mar	64.2	9.8	555.1
Apr	80.7	11.4	607.9
May	109.5	18.2	501.6
Jun	126.4	292	-56.7
Jul	59.7	56.9	4.9
Aug	32.9	55.7	-40.9
Sep	-0.2	45.5	-100.4
Oct	-4.9	32.6	-115.0
Nov	5.9	18.2	-67.6
Dec	32.1	11.5	179.1
Sum	620.4	570.0	8.85

Figure 5-17: Comparison of the mean annual calculated runoff from satellite estimate against the in-situ measurements (Robs) at Cuntan Gauging station from 2005-2010.

Several reasons could have contributed to the lack of closure and are briefly explained. First, the water balance closure was assessed using in-situ and satellite estimates sourced from various satellites, operating at different spatial scale and running on different algorithms. Inherent errors in the individual products could have caused lack of closure in the monthly and annual basin water balance. Secondly, it could be due to unaccounted groundwater leakage to depressions in the basin as the catchment watershed boundary and aquifer extent are not well defined. The assumption that the groundwater component coincided with the watershed boundary, over a closed basin is over-simplistic. Thirdly, the $1^{\circ}\times 1^{\circ}$ GRACE product is spatially coarser than the $0.05^{\circ}\times 0.05^{\circ}$ datasets. Despite resampling to adapt to the research, scale mismatches are intrinsic and contribute to lack of closure. Fourth, the Cuntan station is about 600km from the outflow gates of the dam. Thus, the outflow R (calc) might have been overestimated or may not have been accurately captured. Lastly, unlike the R(calc) that is calculated from spatial averages of satellite inputs (with different spectral characteristics), R(obs) are point measurements with a quicker response than the calculated runoff. Due to differences in satellite overpasses and dam-operation regimes, the spikes appear to have been missed in the R(calc) series although they are intrinsically included. Thus, the R(calc) peaks are not spiky as the R(obs) series. To accurately estimate runoff, incorporation of a hydrological model coupled with a digital elevation model is necessary.

In summary, from Figure 5-16, the R(calc) series has a distinct pattern. The R(calc) has a deficit of approximately 20mm in late 2005 (Sept-Dec), a recurrence of a similar magnitude event is in 2008 (Sept-Dec) with a deficit of approximately -25mm. Similarly, a smaller magnitude event, of ~ -10 mm occurring in 2007 (Oct-Dec) reappears in late 2010 (Oct-Dec). A drop in the peak discharge of R(obs) series in subsequent years is also observed, i.e., the peak discharge in the R(obs) dropped from 340mm in 2005 to 280mm in 2006 and from 300mm to 260mm in 2009 suggesting reduced dam-water release in the years; probably as a result of drought or over abstraction upstream. Interestingly, the years 2006, 2009/2011 are reported as drought years. Whether this is coincidental, needs further exploration. Otherwise, water balance can infer drought tendencies and repeat cycles and would support (Su, He et al., 2017) recommendation to incorporate the water balance to study hydrological drought.

6. CONCLUSION

The objectives of this research were to assess the efficacy and the consistency of four standardized drought indices in describing a drought event, assess at what timescale/length drought should be monitored and understand relevance of the water balance in monitoring hydrological drought in order to overcome inconsistencies in drought monitoring.

In determining SPEI, a modified approach introduced by Homdee et al. (2016) was applied instead. The SPAEI results compared to existing SPEI database imagery seem to depict good agreement and reliability as in seen Figure 5-5. Four of the five indices, the SPI, SPAEI, SVI and the STWSI were used for analysis premised upon CHIRPS rainfall product, SEBS ETa, MODIS NDVI and GRACE TWS. The water balance approach was also used to assess the hydrological drought at a catchment scale.

- The results show that the proposed framework is feasible and can offer integral insights as regards drought monitoring as it holistically addresses different components of the water cycle. Standardization ensures compatibility and comparability and suppresses variations. However, there are constraints due to scale issues, data inconsistencies and data availability; standardization procedure notwithstanding.
- From the study, SPAEI was found to have higher severity and longer drought durations compared to SPI, probably because the SPAEI incorporates ETa. Both the SPI and SPAEI respond well to changes in precipitation and are able to pick drought events consistently. All the four indices depicted a strong agreement at longer time-steps (i.e. >6 months), and is highest at the 9-months' time steps for SPI and SPAEI. As a result, we can conclude that drought monitoring can effectively be monitored at 6-9months scale.
- SPI and SPAEI are suitable to monitor meteorological drought as infer changes occurring at shallow depth and on surface. STWSI tracks deep water horizons and the TWS. Thus STWSI and SPAEI can complement each other in monitoring hydrological drought. SVI is limited and should be used in conjunction with other drought indices as it is affected by phenology and other meteorological forcing.
- The water balance does not close probably due spatial scale mismatch and due errors inherent to the data, satellite products, observations and spatial heterogeneity within the catchment. However, despite lack of closure, the difference between the accumulated annual R(calc) and R(obs) is minimal (620mm against 570mm) and the mean bias error in the annual runoff was 8.85% although larger on month-month.
- The Three Gorges Dam is a fully regulated (operated) dam. As a check against floods and to create room for the upstream reservoir, water is released from the dam in June. There is possibly exchange between the ETa and the groundwater such that groundwater replenishes storage deficits in winter when the ground is frozen and is preferentially released to fill up the TGB dam in summer. The consequence of is that calculated runoff overestimates runoff in winter through summer except for June where the observed runoff is twice the calculated runoff due to the dam-water release.
- As explained in section 5.5, the deficits in the water balance estimation appear to have a cyclic repeat cycle occurring just before (coincide with) reported drought events. Notably, amount of water released from the Three Gorge Dam appears to be less than normal observed discharges

following the deficit. If not coincidental, this confirms Su et al. (2017) assertion that, the water balance can infer drought.

6.1. Recommendations:

- The standardized drought framework is feasible, especially with indices using similar inputs such as the SPI, SPEI/SPA EI and STWSI. However, there are limitations with NDVI-based indices as do not respond to metrological influences. Future research may incorporate alternatives non-DVI NDVI agricultural drought indices.
- More research is needed to ascertain whether the re-occurrence of the deficits in the water balance solution is coincidental or not. Future research to incorporate an appropriate hydrological model integrating catchment characteristics and soil moisture measurements for better characterization.

LIST OF REFERENCES

- Anyadike, O. (2017). IRIN | Drought in Africa 2017. Retrieved June 1, 2017, from <https://www.irinnews.org/feature/2017/03/17/drought-africa-2017>
- Anyamba, A., & Tucker, C. J. (2012). Historical Perspectives on AVHRR NDVI and Vegetation Drought Monitoring. In *Remote Sensing of Drought* (pp. 23–50). <https://doi.org/doi:10.1201/b11863-4>
- Beguéría, S., Vicente-Serrano, S. M., Reig, F., & Latorre, B. (2014). Standardized precipitation evapotranspiration index (SPEI) revisited: Parameter fitting, evapotranspiration models, tools, datasets and drought monitoring. *International Journal of Climatology*, *34*(10), 3001–3023. <https://doi.org/10.1002/joc.3887>
- C, R. E., Restrepo, J. D., Brakenridge, G. R., & Kettner, A. J. (2017). Remote Sensing of Hydrological Extremes. In *Remote Sensing of Hydrological Extremes* (pp. 151–172). <https://doi.org/10.1007/978-3-319-43744-6>
- Chen, J., Finlayson, B. L., Wei, T., Sun, Q., Webber, M., Li, M., & Chen, Z. (2016). Changes in monthly flows in the Yangtze River, China - With special reference to the Three Gorges Dam. *Journal of Hydrology*, *536*, 293–301. <https://doi.org/10.1016/j.jhydrol.2016.03.008>
- Chen, X., Su, Z., Ma, Y., Liu, S., Yu, Q., & Xu, Z. (2014). Development of a 10-year (2001–2010) 0.1° data set of land-surface energy balance for mainland China. *Atmospheric Chemistry and Physics*, *14*(23), 13097–13117. <https://doi.org/10.5194/acp-14-13097-2014>
- Deng, G., Li, L., & Song, Y. (2016). Provincial water use efficiency measurement and factor analysis in China: Based on SBM-DEA model. *Ecological Indicators*, *69*, 12–18. <https://doi.org/10.1016/j.ecolind.2016.03.052>
- FAO, IFAD, UNICEF, WFP, & WHO. (2017). The state of food security and nutrition in the world 2017. building resilience for peace and food security. *Fao*, 117. Retrieved from <http://www.fao.org/3/a-I7695e.pdf>
- Forootan, E., Safari, A., Mostafaie, A., Schumacher, M., Delavar, M., & Awange, J. L. (2017, May 1). Large-Scale Total Water Storage and Water Flux Changes over the Arid and Semiarid Parts of the Middle East from GRACE and Reanalysis Products. *Surveys in Geophysics*. Springer Netherlands. <https://doi.org/10.1007/s10712-016-9403-1>
- Funk, C., Peterson, P., Landsfeld, M., Pedreros, D., Verdin, J., Shukla, S., ... Michaelsen, J. (2015). The climate hazards infrared precipitation with stations - A new environmental record for monitoring extremes. *Scientific Data*, *2*, 150066. <https://doi.org/10.1038/sdata.2015.66>
- Heim, R. R. (2002). A review of twentieth-century drought indices used in the United States. *Bulletin of the American Meteorological Society*, *83*(8), 1149–1165. [https://doi.org/10.1175/1520-0477\(2002\)083<1149:AROTDI>2.3.CO;2](https://doi.org/10.1175/1520-0477(2002)083<1149:AROTDI>2.3.CO;2)
- Helsel, D. R., & Hirsch, R. M. (1995). Statistical Methods in Water Resources. Retrieved from <https://pubs.usgs.gov/twri/twri4a3/pdf/twri4a3-new.pdf>
- Hennemuth, B., Bender, S., Bulow, K., Dreier, N., Keup-Thiel, E., Kruger, O., ... Schoetter, R. (2013). CSC Report 13 Statistical methods for the analysis of simulated and observed climate data Applied in projects and institutions dealing with climate change impact and adaptation. *CSC Report, Climate Service Center, Germany*, *13*, 138. Retrieved from http://epub.sub.uni-hamburg.de/epub/volltexte/2013/23973/pdf/csc_report13_englisch_final_mit_umschlag.pdf
- Homdee, T., Pongput, K., & Kanae, S. (2016). A comparative performance analysis of three standardized climatic drought indices in the Chi River basin, Thailand. *Agriculture and Natural Resources*, *50*(3), 211–219. <https://doi.org/10.1016/j.anres.2016.02.002>
- Hook, L. (2011, May 24). China faces worst drought in 50 years. *Financial Times*, p. A70. Retrieved from <https://www.ft.com/content/7d6e4db8-861e-11e0-9e2c-00144feabdc0>
- Huang, Y., Salama, M. S., Krol, M. S., Su, Z., Hoekstra, A. Y., Zeng, Y., & Zhou, Y. (2015). Estimation of human-induced changes in terrestrial water storage through integration of GRACE satellite detection and hydrological modeling: A case study of the Yangtze River basin. *Water Resources Research*, *51*(10), 8494–8516. <https://doi.org/10.1002/2015WR016923>
- Huang, Y., Salama, M. S., Krol, M. S., Van Der Velde, R., Hoekstra, A. Y., Zhou, Y., & Su, Z. (2013). Analysis of long-term terrestrial water storage variations in the Yangtze River basin. *Hydrology and Earth System Sciences*, *17*(5), 1985–2000. <https://doi.org/10.5194/hess-17-1985-2013>

- Huang Wei. (2017). The worst drought ever recorded in northern China - The New York Times Chinese website. *New York Times*. Retrieved from <https://cn.nytimes.com/china/20170630/china-drought/?action=click&contentCollection=Asia-Pacific&module=Translations®ion=Header&version=zh-CN&ref=en-US&pgtype=article>
- Husak, G. J., Michaelsen, J., & Funk, C. (2007). Use of the gamma distribution to represent monthly rainfall in Africa for drought monitoring applications. *International Journal of Climatology*, 27(7), 935–944. <https://doi.org/10.1002/joc.1441>
- Iglesias, A., Cancelliere, A., Wilhite, D. A., Garrote, L., & Cubillo, F. (2009). *Coping with Drought Risk in Agriculture and Water Supply Systems*. (A. Iglesias, A. Cancelliere, D. A. Wilhite, L. Garrote, & F. Cubillo, Eds.). Dordrecht: Springer Netherlands. <https://doi.org/10.1007/978-1-4020-9045-5>
- Jain, V. K., Pandey, R. P., Jain, M. K., & Byun, H. R. (2015). Comparison of drought indices for appraisal of drought characteristics in the Ken River Basin. *Weather and Climate Extremes*, 8, 1–11. <https://doi.org/10.1016/j.wace.2015.05.002>
- Jiang, D., Wang, J., Huang, Y., Zhou, K., Ding, X., & Fu, J. (2014, June 5). The review of GRACE data applications in terrestrial hydrology monitoring. *Advances in Meteorology*. Hindawi. <https://doi.org/10.1155/2014/725131>
- Kogan, F. N. (1990). Remote sensing of weather impacts on vegetation in non-homogeneous areas. *International Journal of Remote Sensing*, 11(8), 1405–1419. <https://doi.org/10.1080/01431169008955102>
- Liu, B., Xu, M., Henderson, M., Qi, Y., & Li, Y. (2004). Taking China's temperature: Daily range, warming trends, and regional variations, 1955-2000. *Journal of Climate*, 17(22), 4453–4462. <https://doi.org/10.1175/3230.1>
- Long, D., Longuevergne, L., & Scanlon, B. R. (2015). Global analysis of approaches for deriving total water storage changes from GRACE satellites. *Water Resources Research*, 51(4), 2574–2594. <https://doi.org/10.1002/2014WR016853>
- Maccherone, B. (2014). MODIS Web. *MODIS Web*. Retrieved from <https://modis.gsfc.nasa.gov/data/>
- Mckee, T. B., Doesken, N. J., & Kleist, J. (1993). The relationship of drought frequency and duration to time scales. In Department of Atmospheric Science (Ed.), *AMS 8th Conference on Applied Climatology* (pp. 179–184). Anaheim, California: Colorado State University. <https://doi.org/citeulike-article-id:10490403>
- Moriasi, D. N., J. G. Arnold, M. W. Van Liew, R. L. Bingner, R. D. Harmel, & T. L. Veith. (2007). Model Evaluation Guidelines for Systematic Quantification of Accuracy in Watershed Simulations. *Transactions of the ASABE*, 50(3), 885–900. <https://doi.org/10.13031/2013.23153>
- Nagarajan, R. (2010). Spatial Data and Geographical Information System. In *Drought Assessment* (pp. 265–319). Dordrecht: Springer Netherlands. https://doi.org/10.1007/978-90-481-2500-5_7
- Narasimhan, B., & Srinivasan, R. (2005). Development and evaluation of Soil Moisture Deficit Index (SMDI) and Evapotranspiration Deficit Index (ETDI) for agricultural drought monitoring. In *Agricultural and Forest Meteorology* (Vol. 133, pp. 69–88). <https://doi.org/10.1016/j.agrformet.2005.07.012>
- Niemeyer, S. (2008). New drought indices. *Options Méditerranéennes*, 80(80), 267–274. <https://doi.org/10.1017/CBO9781107415324.004>
- OMT. (2012). *Global report on food tourism*. Food Security Information Network. Retrieved from http://cf.cdn.unwto.org/sites/all/files/pdf/global_report_on_food_tourism.pdf
- Palmer, W. C. (1965). Meteorological Drought. *U.S. Weather Bureau, Res. Pap. No. 45*. Retrieved from <https://www.ncdc.noaa.gov/temp-and-precip/drought/docs/palmer.pdf>
- Peng, J., Loew, A., Chen, X., Ma, Y., & Su, Z. (2016). Comparison of satellite-based evapotranspiration estimates over the Tibetan Plateau. *Hydrology and Earth System Sciences*, 20(8), 3167–3182. <https://doi.org/10.5194/hess-20-3167-2016>
- Peters, A. J., Waltershea, E. A., Lel JI, A. V., Hayes, M. M., Svoboda, M. D., Ji, L. L., ... Svoboda, M. D. (2002). Drought monitoring with NDVI-based standardized vegetation index. *American Society for Photogrammetry and Remote Sensing*, 68(1), 71–75. <https://doi.org/0099-1112/02/6800-07>
- Potopová, V., Štěpánek, P., Možný, M., Türkott, L., & Soukup, J. (2015). Performance of the standardised precipitation evapotranspiration index at various lags for agricultural drought risk assessment in the Czech Republic. *Agricultural and Forest Meteorology*, 202, 26–38. <https://doi.org/10.1016/j.agrformet.2014.11.022>
- Qian, M., Zheng-Hui, X., & Lin-Na, Z. (2010). Variations of Terrestrial Water Storage in the Yangtze River Basin under Climate Change Scenarios. *Atmospheric and Oceanic Science Letters*, 3(6), 293–298. <https://doi.org/10.1080/16742834.2010.11446885>

- Raziei, T., Martins, D. S., Bordi, I., Santos, J. F., Portela, M. M., Pereira, L. S., & Sutera, A. (2015). SPI Modes of Drought Spatial and Temporal Variability in Portugal: Comparing Observations, PT02 and GPCP Gridded Datasets. *Water Resources Management*, 29(2), 487–504. <https://doi.org/10.1007/s11269-014-0690-3>
- Richey, A. S., Thomas, B. F., Lo, M.-H., Famiglietti, J. S., Swenson, S., & Rodell, M. (2015). Uncertainty in global groundwater storage estimates in a Total Groundwater Stress framework. *Water Resources Research*, 51(7), 5198–5216. <https://doi.org/10.1002/2015WR017351>
- Rodell, M., & Famiglietti, J. S. (2001). An analysis of terrestrial water storage variations in Illinois with implications for the Gravity Recovery and Climate Experiment (GRACE). *Water Resources Research*, 37(5), 1327–1339. <https://doi.org/10.1029/2000WR900306>
- Stagge, J. H., Tallaksen, L. M., Gudmundsson, L., & Loon, F. Van. (2015). Candidate Distributions for Climatological Drought Indices (SPI and SPEI). *International Journal of Climatology*, 40(40)(February), 4027–4040. <https://doi.org/10.1002/joc.4267>
- Stagge, J. H., Tallaksen, L. M., Gudmundsson, L., Van Loon, A. F., & Stahl, K. (2016). Response to comment on “Candidate Distributions for Climatological Drought Indices (SPI and SPEI).” *International Journal of Climatology*, 36(4), 2132–2138. <https://doi.org/10.1002/joc.4564>
- Strassberg, G., Scanlon, B. R., & Chambers, D. (2009). Evaluation of groundwater storage monitoring with the GRACE satellite: Case study of the High Plains aquifer, central United States. *Water Resources Research*, 45(5). <https://doi.org/10.1029/2008WR006892>
- Su, Z. (2002). The Surface Energy Balance System (SEBS) for estimation of turbulent heat fluxes. *Hydrology and Earth System Sciences*, 6(1), 85–100. <https://doi.org/10.5194/hess-6-85-2002>
- Su, Z., He, Y., Dong, X., & Wang, L. (2017). Remote Sensing of Hydrological Extremes. In *Remote Sensing of Hydrological Extremes* (pp. 151–172). <https://doi.org/10.1007/978-3-319-43744-6>
- Su, Z., Timmermans, W., Zeng, Y., Schulz, J., John, V. O., Roebeling, R. A., ... Wen, J. (2017). An overview of European efforts in generating climate data records. *Bulletin of the American Meteorological Society*, BAMS-D-16-0074.1. <https://doi.org/10.1175/BAMS-D-16-0074.1>
- Suliman, A. H. A., Jajarmizadeh, M., Harun, S., & Mat Darus, I. Z. (2015). Comparison of Semi-Distributed, GIS-Based Hydrological Models for the Prediction of Streamflow in a Large Catchment. *Water Resources Management*, 29(9), 3095–3110. <https://doi.org/10.1007/s11269-015-0984-0>
- Sun, Q., Miao, C., & Duan, Q. (2015). Projected changes in temperature and precipitation in ten river basins over China in 21st century. *International Journal of Climatology*, 35(6), 1125–1141. <https://doi.org/10.1002/joc.4043>
- Swenson, S., & Wahr, J. (2006). Post-processing removal of correlated errors in GRACE data. *Geophysical Research Letters*, 33(8), L08402. <https://doi.org/10.1029/2005GL025285>
- Tapley, B. D., Bettadpur, S., Watkins, M., & Reigber, C. (2004). The gravity recovery and climate experiment: Mission overview and early results. *Geophysical Research Letters*, 31(9), n/a-n/a. <https://doi.org/10.1029/2004GL019920>
- USGS. (2012). *Science for a changing world*. Milford, Pennsylvania: USGS. Retrieved from <https://pubs.usgs.gov/wri/2000/4112/report.pdf>
- Vicente-Serrano, S. M., Beguerua, S., & Lopez-Moreno, J. I. (2010). SPEI Global Drought Monitor. Retrieved May 22, 2017, from <http://spei.csic.es/map/maps.html#months=1%23month=3%23year=2017>
- Vicente-Serrano, S. M., Lopez-Moreno, J. I., Beguería, S., Lorenzo-Lacruz, J., Sanchez-Lorenzo, A., García-Ruiz, J. M., ... Espejo, F. (2014). Evidence of increasing drought severity caused by temperature rise in southern Europe. *Environmental Research Letters*, 9(4), 44001. <https://doi.org/10.1088/1748-9326/9/4/044001>
- Vicente-Serrano, S., & López-Moreno, J. I. (2010). A multiscale drought index sensitive to global warming: The standardized precipitation evapotranspiration index. *Journal of Climate*, 23(7), 1696–1718. <https://doi.org/10.1175/2009JCLI2909.1>
- Vicente-Serrano, J. I., López-Moreno, J. I., Gimeno, L., Nieto, R., Morán-Tejeda, E., Lorenzo-Lacruz, J., ... Azorin-Molina, C. (2011). A multiscale global evaluation of the impact of ENSO on droughts. *Journal of Geophysical Research Atmospheres*, 116(20), D20109. <https://doi.org/10.1029/2011JD016039>
- Wang, W., Ertsen, M. W., Svoboda, M. D., & Hafeez, M. (2016, March 23). Propagation of drought: From meteorological drought to agricultural and hydrological drought. *Advances in Meteorology*. Hindawi. <https://doi.org/10.1155/2016/6547209>
- Wang, Y., Liu, B., Su, B., Zhai, J., & Gemmer, M. (2011). Trends of calculated and simulated actual

- evaporation in the Yangtze River Basin. *Journal of Climate*, 24(16), 4494–4507.
<https://doi.org/10.1175/2011JCLI3933.1>
- Wilhite, D. A., & Glantz, M. H. (1985). Understanding the Drought Phenomenon: The Role of Definitions. *Water International*, 10(3), 111–120. Retrieved from
<http://digitalcommons.unl.edu/droughtfacpub>
- Wilhite, D. A., Svoboda, M. D., & Hayes, M. J. (2007). Understanding the complex impacts of drought: A key to enhancing drought mitigation and preparedness. *Water Resources Management*, 21(5), 763–774.
<https://doi.org/10.1007/s11269-006-9076-5>
- Wilks, D. S. (1990). Maximum Likelihood Estimation for the Gamma Distribution Using Data Containing Zeros. *Journal of Climate*, 3(12), 1495–1501. [https://doi.org/10.1175/1520-0442\(1990\)003<1495:MLEFTG>2.0.CO;2](https://doi.org/10.1175/1520-0442(1990)003<1495:MLEFTG>2.0.CO;2)
- Xu, K., Yang, D., Yang, H., Li, Z., Qin, Y., & Shen, Y. (2015). Spatio-temporal variation of drought in China during 1961–2012: A climatic perspective. *Journal of Hydrology*, 526, 253–264.
<https://doi.org/10.1016/j.jhydrol.2014.09.047>
- Yang, P., Xiao, Z., Yang, J., & Liu, H. (2013). Characteristics of clustering extreme drought events in China during 1961–2010. *Acta Meteorologica Sinica*, 27(2), 186–198. <https://doi.org/10.1007/s13351-013-0204-x>
- Yang, S. L., Liu, Z., Dai, S. B., Gao, Z. X., Zhang, J., Wang, H. J., ... Zhang, Z. (2010). Temporal variations in water resources in the Yangtze River (Changjiang) over the Industrial Period based on reconstruction of missing monthly discharges. *Water Resources Research*, 46(10).
<https://doi.org/10.1029/2009WR008589>
- Yu, M., Li, Q., Hayes, M. J., Svoboda, M. D., & Heim, R. R. (2014). Are droughts becoming more frequent or severe in China based on the standardized precipitation evapotranspiration index: 1951–2010? *International Journal of Climatology*, 34(3), 545–558. <https://doi.org/10.1002/joc.3701>
- Yurekli, K., & Kurunc, A. (2006). Simulating agricultural drought periods based on daily rainfall and crop water consumption. *Journal of Arid Environments*, 67(4), 629–640.
<https://doi.org/10.1016/j.jaridenv.2006.03.026>
- Zargar, A., Sadiq, R., Naser, B., & Khan, F. I. (2011). A review of drought indices. *Environmental Reviews*, 19(NA), 333–349. <https://doi.org/10.1139/a11-013>
- Zhai, P., Zhang, X., Wan, H., & Pan, X. (2005). Trends in total precipitation and frequency of daily precipitation extremes over China. *Journal of Climate*, 18(7), 1096–1108.
<https://doi.org/10.1175/JCLI-3318.1>
- Zhang, L., Chen, X., Cai, X., & Salim, H. A. (2010). Spatial-temporal changes of NDVI and their relations with precipitation and temperature in Yangtze river basin from 1981 to 2001. *Geo-Spatial Information Science*, 13(3), 186–190. <https://doi.org/10.1007/s11806-010-0339-1>
- Zhang, Q., Jiang, T., Gemmer, M., & Becker, S. (2005). Precipitation, temperature and runoff analysis from 1950 to 2002 in the Yangtze basin, China. *Hydrological Sciences—Journal—des Sciences Hydrologiques*, 50(August). Retrieved from
<http://citeseerx.ist.psu.edu/viewdoc/download?doi=10.1.1.726.6021&rep=rep1&type=pdf>

APPENDICES

Appendix 1: Correlation matrix (Part 1)

	SPI -1	SPI -3	SPI -6	SPI -9	SPI- 12	SPI- 24	SPAE I-1	SPAEI -3	SPAEI -6	SPAEI -9	SPAEI -12	SPAEI- 24
SPI-1	1											
SPI-3	0.61	1										
SPI-6	0.43	0.7	1									
SPI-9	0.3	0.54	0.79	1								
SPI-12	0.2	0.4	0.65	0.87	1							
SPI-24	0.28	0.44	0.6	0.69	0.69	1						
SPAEI-1	0.87	0.54	0.47	0.36	0.25	0.3	1					
SPAEI-3	0.52	0.89	0.7	0.6	0.47	0.49	0.59	1				
SPAEI-6	0.41	0.65	0.96	0.8	0.69	0.65	0.48	0.73	1			
SPAEI-9	0.3	0.52	0.77	0.97	0.85	0.73	0.38	0.62	0.83	1		
SPAEI-12	0.21	0.41	0.65	0.86	0.97	0.73	0.27	0.49	0.72	0.88	1	
SPAEI-24	0.25	0.38	0.56	0.63	0.61	0.93	0.27	0.43	0.6	0.69	0.7	1
SVI-1	0.33	0.39	0.4	0.43	0.73	0.46	0.36	0.48	0.44	0.45	0.45	0.47
SVI-3	0.23	0.4	0.44	0.45	0.44	0.47	0.27	0.47	0.5	0.49	0.47	0.5
SVI-6	0.19	0.3	0.45	0.48	0.45	0.51	0.28	0.42	0.52	0.53	0.51	0.55
SVI-9	0.18	0.32	0.42	0.49	0.48	0.55	0.28	0.43	0.5	0.54	0.54	0.58
SVI-12	0.21	0.3	0.41	0.47	0.48	0.56	0.29	0.43	0.49	0.52	0.53	0.57
SVI-24	0.22	0.32	0.45	0.51	0.51	0.63	0.3	0.44	0.52	0.56	0.56	0.65
STWS-1	0.25	0.31	0.34	0.41	0.4	0.45	0.34	0.46	0.44	0.42	0.42	0.41
STWS-3	0.03	0.31	0.43	0.48	0.47	0.48	0.12	0.48	0.56	0.52	0.49	0.43
STWS-6	0.14	0.31	0.56	0.62	0.57	0.56	0.18	0.43	0.69	0.67	0.6	0.48
STWS-9	0.06	0.23	0.52	0.7	0.7	0.73	0.09	0.31	0.63	0.76	0.75	0.73
STWS-12	0.03	0.17	0.33	0.56	0.67	0.68	-0.02	0.14	0.39	0.61	0.73	0.76
STWS-24	-0.1	0.12	0.4	0.44	0.38	0.73	0.07	0.24	0.41	0.4	0.33	0.75
Average Cor	0.30	0.44	0.56	0.60	0.58	0.60	0.35	0.51	0.61	0.63	0.59	0.58
Similar step cor	0.61	0.65	0.74	0.79	0.78	0.82	0.61	0.53	0.66	0.72	0.71	0.76

Appendix 2: Correlation matrix (Part 2)

	SVI -1	SVI-3	SVI-6	SVI -9	SVI -12	SVI -24	STW S-1	STW S-3	STW S-6	STW S-9	STWS- 12	STW S-24
SPI-1	0.33	0.23	0.19	0.18	0.21	0.22	0.25	0.03	0.14	0.06	0.03	-0.1
SPI-3	0.39	0.4	0.3	0.32	0.3	0.32	0.31	0.31	0.31	0.23	0.17	0.12
SPI-6	0.4	0.44	0.45	0.42	0.41	0.45	0.34	0.43	0.56	0.52	0.33	0.4
SPI-9	0.43	0.45	0.48	0.49	0.47	0.51	0.41	0.48	0.62	0.7	0.56	0.44
SPI-12	0.73	0.44	0.45	0.48	0.48	0.51	0.4	0.47	0.57	0.7	0.67	0.38
SPI-24	0.46	0.47	0.51	0.55	0.56	0.63	0.45	0.48	0.56	0.73	0.68	0.73
SPAEI-1	0.36	0.27	0.28	0.28	0.29	0.3	0.34	0.12	0.18	0.09	-0.02	0.07
SPAEI-3	0.48	0.47	0.42	0.43	0.43	0.44	0.46	0.48	0.43	0.31	0.14	0.24
SPAEI-6	0.44	0.5	0.52	0.5	0.49	0.52	0.44	0.56	0.69	0.63	0.39	0.41
SPAEI-9	0.45	0.49	0.53	0.54	0.52	0.56	0.42	0.52	0.67	0.76	0.61	0.4
SPAEI- 12	0.45	0.47	0.51	0.54	0.53	0.56	0.42	0.49	0.6	0.75	0.73	0.33
SPAEI- 24	0.47	0.5	0.55	0.58	0.57	0.65	0.41	0.43	0.48	0.73	0.76	0.75
SVI-1	1	0.92	0.83	0.8	0.83	0.82	0.43	0.24	-0.07	-0.06	-0.1	0.03
SVI-3		1	0.93	0.89	0.89	0.88	0.4	0.29	-0.12	-0.08	-0.14	-0.03
SVI-6			1	0.97	0.94	0.93	0.37	0.26	-0.17	-0.14	-0.2	-0.2
SVI-9				1	0.98	0.96	0.4	0.28	-0.23	-0.19	-0.24	-0.36
SVI-12					1	0.98	0.42	0.32	-0.19	-0.17	-0.18	-0.39
SVI-24						1	0.44	0.34	-0.09	-0.06	-0.07	-0.13
STWS-1							1	0.74	0.45	0.27	0.19	0.33
STWS-3								1	0.74	0.56	0.38	0.52
STWS-6									1	0.85	0.65	0.63
STWS-9										1	0.87	0.66
STWS-12											1	0.66
STWS-24												1
Average Cor	0.46	0.46	0.45	0.44	0.45	0.49	0.42	0.44	0.39	0.41	0.33	0.29
Similar step cor	0.53	0.54	0.45	0.46	0.46	0.40	0.51	0.52	0.52	0.57	0.56	0.70

Appendix 3: The SPI MATLAB script

```
%clc
%clear all
%% disp NC data
% ncdisp('D:\CHIRPS_Netcdf\chirps-v2.0.monthly.nc');
tic
%% read precip for china (25N-35N and 90E-120E)
% longitude start from -180 to 180, latitude start from -50 to 50
% precipitation represented on 0.05 x 0.05 degree
% 24N = (24+50)/0.05 = 1480; 35.5N = (35.5+50)/0.05 = 1700
% 90E = (90+180)/0.05 = 5400; 120.5E = (120.5+180)/0.05 = 6010 108.75

fname='D:\CHIRPS_Netcdf\chirps-v2.0.monthly.nc';
lon=ncread(fname,'longitude', 5400, 610, 1);
lat=ncread(fname,'latitude', 1480, 230, 1);
[lat, lon]=meshgrid(lat, lon);
p = ncread(fname,'precip',[5400 1480 1], [610 230 inf], [1 1 1]);% read and subset data to AOI
p=permute(p,[2,1,3]);
t = ncread(fname,'time');%Read the time variable from the netcdf file and convert date to a
numeric array
tm = double(t + datenum('1-jan-1980')); %convert the time variable to Matlab format starting
Jan1980
[y,m] = datevec(tm);%Create numeric date and time vector array whose values represent the date
and time components of years, months, days
in=find(y==2016 & m==12);

%% Moving average P,Calculate scaled precip
nanmap = nan*ones(size(p,1),size(p,2),1);
[p3, p6, p9, p12, p24]=deal(nan*p); %Container array for scaled precipitation variable
temp = movmean(p,3,3);
p3(:,3:end) = temp(:,2:end-1); %Average variable by desired scale and shift it along the scale and
discard endpoints
temp = movmean(p,6,3);
p6(:,6:end) = temp(:,4:end-2);
temp = movmean(p,9,3);
p9(:,9:end) = temp(:,5:end-4);
temp = movmean(p,12,3);
p12(:,12:end) = temp(:,7:end-5);
temp = movmean(p,24,3);
p24(:,24:end) = temp(:,13:end-11);
save ('p24', 'p12', 'p9', 'p6', 'p3', 'p')

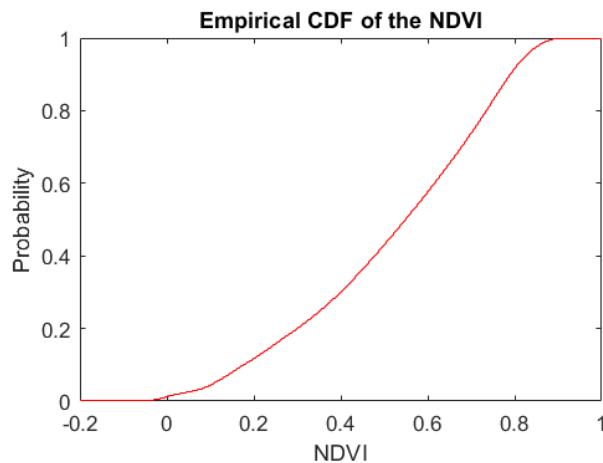
%% Create calculate SPI
[pd,pr,spi] = calcSPI(p,m); %The SPI calculation function
%Call the SPI calculation function and calculate the 3, 6, 12, and 24 month SPI
[pd3,pr3,spi3] = calcSPI(p3,m);
[pd6,pr6,spi6] = calcSPI(p6,m);
[pd9,pr9,spi9] = calcSPI(p9,m);
[pd12,pr12,spi12] = calcSPI(p12,m);
[pd24,pr24,spi24] = calcSPI(p24,m);
save('SPI_updated', 'spi','spi3', 'spi6','spi9','spi12', 'spi24')
```

```

%% SPI Calculation Function
function [pd,pr,spi] = calcSPI(p,m)
spi=NaN*p;
for month = 1:12
    k= find(m==month);
    month
    for row = 1:size(p,2)
    for column = 1:size(p,1)
        pk = p(column,row,k);
        if length(unique(pk(~isnan(pk))))>5 %&& ~isnan(mean(pk)) %ignore values less than 5
            pkn = pk(~isnan(pk));
            pd=fitdist(pkn(:),'gamma'); %fit precip values to a gamma pdf
            pr=cdf(pd, pkn(:)); % cumulative probability
            %if isnan(sum(pr)), keyboard, end
            %if ~isnan(icdf('normal',pr,0,1);%(~isnan(pk))))
                spi(column,row,k(~isnan(pk)))=icdf('normal',pr,0,1);%(~isnan(pk)) %Invert
cumulative probabilities to normal, result SPI
            end
            % plot(cdf(pd,x)), hold on
            % plot(hist(p(row,column,k)));
        end
    end
end
%r=find(isnan(p)); %find NaN in precip
end

```

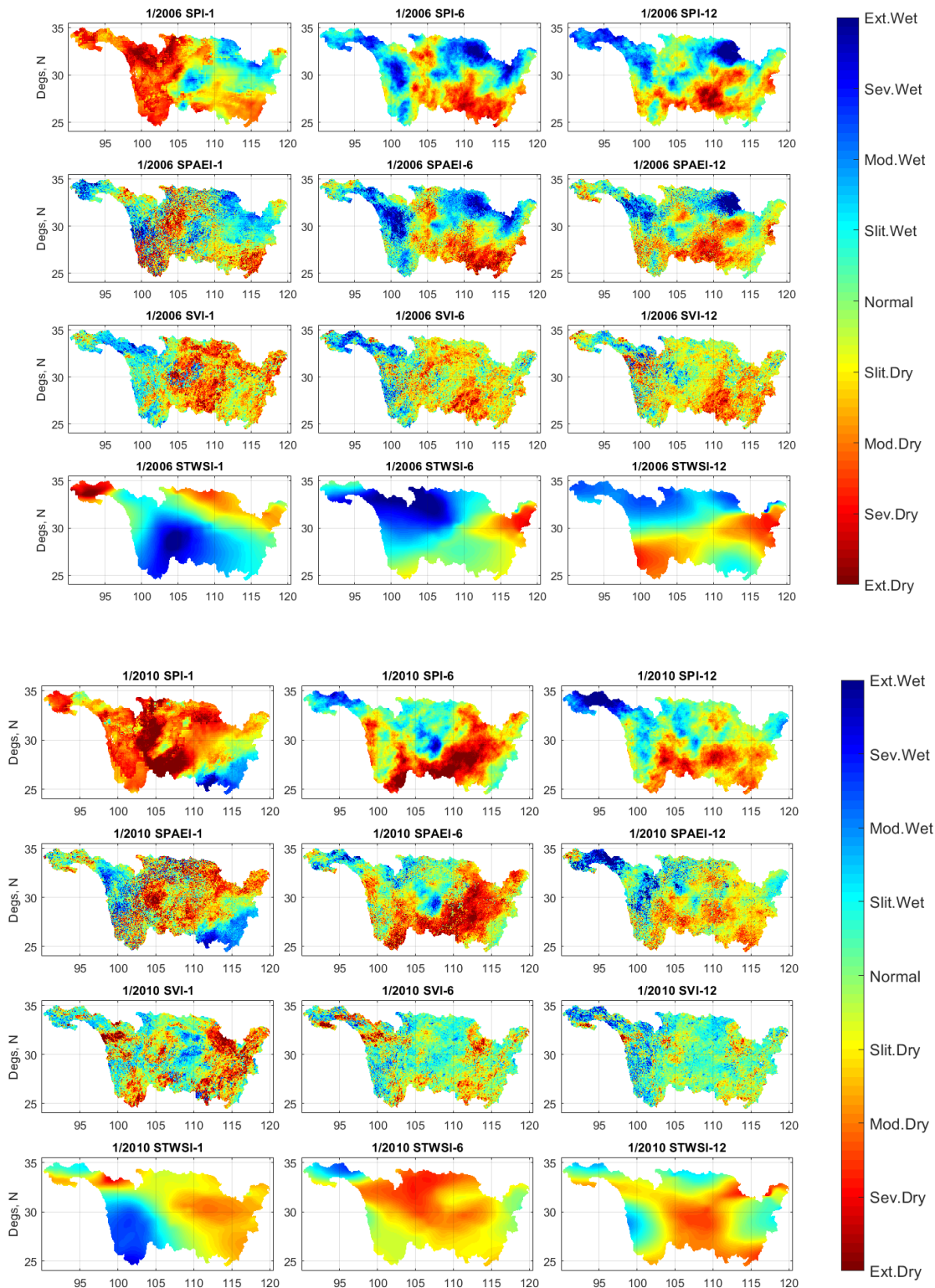
Appendix 4: MODIS NDVI empirical cumulative probability distribution



MODIS Data normalization equation

$$NDVI_{norm} = \frac{NDVI - NDVI_{min}}{NDVI_{max} - NDVI_{min}}$$

Appendix 5: Comparison of drought as captured by the 1, 6 and 12-month indices in January 2006 and January 2010



Appendix 6: Comparison of drought as captured by the 1, 6 and 12-month indices in July 2006 and July 2010

